Ingineria automobilului

Automotive engineering

Registrul Auto Român

SIAR

Societatea Inginerilor de Automobile din România

OFICIAL JOURNAL OF THE SOCIETY OF AUTOMOTIVE ENGINEERS OF ROMANIA – SIAR
SPONSORED BY THE ROMANIAN AUTOMOTIVE REGISTER – RAR OPEN ACCESS

ISSN 1842 – 4074
NR. 79/IUNIE 2026

Kart Low Cost 2026 – Ediția a XIV-a 5 – 7 mai 2026, ISAT de Nevers, Franța













- Programarea încărcării inteligente pentru flotele de vehicule electrice
- Evaluarea comportamentului mecanic și a performanței unui nou concept al casetei de direcție
- Analiza modală și optimizarea structurii cabinei de autocamion
- Analiza beneficiilor privind economia de combustibil și emisiile poluante pentru arhitecturile *Mild Hybrid MHEV* de 48 V (P0-P2)

SIAR ESTE MEMBRĂ FISITA INTERNATIONAL FEDERATION OF AUTOMOTIVE ENGINEERING SOCIETIES

EAEC EUROPEAN AUTOMOBILE ENGINEERS COOPERATION

APARE TRIMESTRIAL
QUARTERLY
FREE OF CHARGE

The 36th International Congress of Automotive and Transport Engineering

MOBILITY ENGINEERING AND SUSTAINABILITY

5 -7 November 2026, Pitești, Romania

ENDORSED BY FISITA

Congress Themes:

1. *Accident Research and Analysis*
2. *Active and Passive Safety*
3. *Advanced Engineering Methods (CAx)*
4. *Advanced Materials, Manufacturing Technologies and Logistics*
5. *Advanced Transport Systems and Road Traffic*
6. *Heavy and Special Vehicles*
7. *Hybrid & Electric Vehicles*
8. *Internal Combustion Engines*
9. *Transmission Systems*
10. *Vehicle Electronics and Software*

The CAR Conference/Congress is a traditional scientific event initiated by University of Pitesti in **1978**. Starting with its 5th edition organized in 1992, CAR International Conference became one of the SIAR Conferences. **CAR Congress reaching its 12th edition this year**, is part of the SIAR's series of similar annual scientific events held successively by various universities in Romania with interests in Automotive Engineering (Transilvania University of Brasov – CONAT Congress, National University of Science and Technology "Politehnica", Bucharest University Center – ESFA Congress, National University of Science and Technology "Politehnica", Pitesti University Center – CAR Congress, Technical University of Cluj-Napoca – AMMA Congress, University of Craiova – SMAT Congress, Polytechnic University of Timisoara – MVT Congress, Moldova Technical University of Chisinau - AITS Congress).
Thus, **CAR2026 is actually the 36th edition of SIAR International Congress.**
The 2026 edition of CAR International Congress is focused on ***MOBILITY ENGINEERING AND SUSTAINABILITY.***
As other SIAR scientific events, **CAR2026** will be an opportunity for delegates to:
- update skills and knowledge by attending focused technical sessions
- gain insights into the automotive industry
- network with potential new partners, clients and suppliers
- view the latest technology products and services in the commercial exhibition

Therefore, academics, researchers, engineers and other specialists in automotive engineering and road transport, students and anyone who is interested are invited to be part of this scientific event. Let us all contribute to its success!

With the support of

SOCIETATEA INGINERILOR DE AUTOMOBILE DIN ROMÂNIA
SOCIETY OF AUTOMOTIVE ENGINEERS OF ROMANIA

Pitești University Center -
National University of Science and Technology POLITEHNICA Bucharest

www.siar.ro
siar@siar.ro

Email: car2026@upit.ro
Website: www.siarcongress.eu
Facebook: https://web.facebook.com/SIAR.CAR/



INITIATIVE VERSUS EXPECTATION
INIȚIATIVĂ VERSUS EXPECTATIVĂ



Depănând amintiri cu un vechi coleg și prieten cu ceva vreme în urmă, la un moment dat am ajuns să aduc în discuție participarea mea la prima manifestare științifică, impresiile puternice remanente și developarea, peste ani, a acelor momente de neuitat. Era în 1980, iar manifestarea științifică era organizată de actuala Universitate Transilvania din Brașov, eu fiind proaspăt absolvent și înscris pentru prezentarea unei lucrări la această „Conferință Națională de Automobile și Tractoare – CONAT 80”! Încurajat fiind de conducătorul proiectului meu de diplomă – regretatul general de brigadă prof. univ. dr. ing. Ioan FILIP (un maramureșean adevărat!), m-am înscris cu o lucrare ce descria conceperea, elaborarea, testarea și validarea unui soft specializat în optimizarea cutiilor de viteze planetare cu două grade de mobilitate cu mecanisme planetare de tip EI. Era o sinteză a proiectului de diplomă în care, printre altele, pe lângă studierea, înțelegerea și aplicarea teoriei grafurilor în rezolvarea temei de proiect, am aplicat programarea structurată – concept inovativ la acea dată!

Dar, nu acesta este subiectul de pus în evidență în acest editorial! O conferință națională remarcabilă deja (la acel moment), organizată de una dintre cele trei universități ce formau ingineri de autovehicule în România, la care un tânăr inginer prezintă rezultatele muncii sale de cercetare-inovare! Subiectul acestui editorial este legat de atmosfera existentă pe durata lucrărilor CONAT 80! A fi un tânăr absolvent în fața celor mai cunoscuți profesori din România în domeniul ingineriei autovehiculelor la acel moment nu era doar o secvență într-un scenariu oarecare – era, cumva, un „ritual de trecere”! Pășind pragul dintre pozițiile de student și absolvent, prezența în fața unei comisii a CONAT 80 era mai mult decât un examen! Era „o confirmare” – dacă era cazul!

Această lungă introducere încearcă să scoată în evidență rolul determinat al comunității academice din domeniul ingineriei autovehiculelor din acea vreme din România în a „valida” munca și rezultatele tinerilor, în a le insufla încredere, în a-i încuraja în împlinirea lor profesională!

Atitudinea colegială, atmosfera călduroasă, mediul cu totul special creat pentru a încuraja tinerii în prezentarea lucrărilor lor era, de fapt, efectul unei înțelegeri – cred eu – depline a rolului de „dascăl” și „mentor” al profesorului în universitate! Tânăr fiind și debutant pe drumul consacrării în profesie, „maeștrii” urmăreau cu înțelegere, curiozitate și discernământ, dar și cu disponibilitatea de a sprijini parcursul unui viitor specialist – posibil viitor cadru didactic universitar!

Așadar, expun situația în care evaluarea și validarea competențelor profesionale în domeniul ingineriei autovehiculelor era de fapt un proces prin care tinerii „aspiranți” erau prezentați „maeștrilor”, cu profilul, munca și rezultatele lor. Încet, urmare a trecerii succesive prin sitele unor astfel de manifestări se obținea „confirmarea”! Recunoașterea profesională presupunea acumulare și confirmare! Succesiva prezență în fața maeștrilor permitea „confirmarea”!

Conceptual, situația actuală este total diferită întrucât accentul pare a fi de tip „contabilicesc”! Criteriile de evaluare și acceptanță în devenirea profesională sunt centrate pe înscrisuri ce probează „vizibilitatea internațională”! Tenace fiind, ascuns în fața unui monitor, acoperind pagini după pagini, publicate pe meridianele lumii, trec etapă după etapă, urc trepte după trepte – uneori fără a fi văzut la față de colegii de breaslă! (Nu că tema ar fi un specific al domeniului nostru!) Fără a elimina acest criteriu, consider că prioritatea ar trebui schimbată. Și atunci, ne-am putea pune întrebarea: ar fi oportună o **inițiativă** în urma căreia „confirmarea” în breaslă să fie rezultatul „expunerii” în fața „maeștrilor”! Congresele SIAR – precum pe vremuri CONAT și nu numai – sunt cadrul potrivit de manifestare pentru tinerii pasionați de domeniul ingineriei autovehiculelor. Este evident că în cadrul puternic reglementat de astăzi această **inițiativă** ar trebui să aparțină „maeștrilor” prin impunerea unui „ritual de trecere”! Ar fi posibil?

Aș vrea să cred că „maeștrii” de astăzi se pot apleca asupra acestei teme și și-ar putea asuma o asemenea responsabilitate! Sau vor rămâne într-o deplină și comodă **expectativă**?

Speranța moare ultima!

Prof. univ. emerit dr. ing. Minu MITREA
Secretar General SIAR

SUMAR „INGINERIA AUTOMOBILULUI“ NR. 79

3 INITIATIVE VERSUS EXPECTATION
INIȚIATIVĂ VERSUS EXPECTATIVĂ
5 SMART CHARGING SCHEDULING FOR EV FLEETS USING REINFORCEMENT LEARNING: BALANCING GRID LOAD, BUSINESS COST, AND CARBON FOOTPRINT
PROGRAMAREA ÎNCĂRCĂRII INTELIGENTE PENTRU FLOTELE DE VEHICULE ELECTRICE UTILIZÂND ÎNVĂȚAREA PRIN CONSOLIDARE: ECHILIBRAREA ÎNCĂRCĂRII REȚELEI, A COSTURILOR DE AFACERI ȘI A AMPRENTEI DE CARBON
10 THE EVALUATION OF THE MECHANICAL BEHAVIOR AND PERFORMANCE OF A NEW STEERING RACK GEOMETRY
EVALUAREA COMPORTAMENTULUI MECANIC ȘI A PERFORMANȚEI UNUI NOU CONCEPT CONSTRUCTIV AL CASETEI DE DIRECȚIE
15 MODAL ANALYSIS AND OPTIMIZATION OF TRUCK CABIN STRUCTURE
ANALIZA MODALĂ ȘI OPTIMIZAREA STRUCTURII CABINEI DE AUTOCAMION
19 FUEL ECONOMY AND CO2 EMISSION BENEFITS OF 48 V MILD HYBRID ARCHITECTURES (P0–P2)
ANALIZA BENEFICIILOR PRIVIND ECONOMIA DE COMBUSTIBIL ȘI EMISIILE POLUANTE PENTRU ARHITECTURILE *MILD HYBRID* MHEV DE 48 V (P0–P2)
25 KART LOW COST 2026

Foto coperta 1: Adrian-Constantin CLENCI

REGISTRUL AUTO ROMÂN

Director general
Mihai ALECU
Director tehnic
Ing. Cristian Viorel BUCUR

Şef Departament Comunicare şi Redacţie Site Auto Test
Roxana DIMA

Redactori
Sorin BARBU
Emilia PETRE

Contact:
Calea Griviţei 391 A,
sector 1, cod poştal 010719,
Bucureşti, România
Tel/Fax: 021/202.70.00
E-mail: autotest@rarom.ro
www.rarom.ro
www.autotestmagazin.ro

SIAR

Contact
Facultatea de Transporturi
UNST Politehnica Bucureşti
Splaiul Independenţei 313
Sala JC005 Cod poştal 060042
Sector 6 Bucureşti România
Tel.: +40.753.081.851
E-mail: siar@siar.ro
VAT Number/CIF 5496135
www.siar.ro
https://www.facebook.com/SIAR.FISITA/
https://www.linkedin.com/company/siar-ro
https://www.linkedin.com/groups

TIPAR
S.C. ART LINES GROUP LTD S.R.L.
Str. Oastei nr. 21,
Bucureşti

The authors declare that the material being presented in the papers is original work, and does not contain or include material taken from other copyrighted sources. Wherever such material has been included, it has been clearly indented or/and identified by quotation marks and due and proper acknowledgements given by citing the source at appropriate places. The views expressed in the articles are those of the authors and are not necessarily endorsed by the publisher. While every case has been taken during production, the publisher does not accept any liability for errors that may have occurred.

EXEMPLAR GRATUIT

SOCIETATEA INGINERILOR DE AUTOMOBILE DIN ROMÂNIA

Cunoaştere şi dezvoltare, prin cooperare! Knowledge and Development by Cooperation!

Preşedinte: Prof. dr. ing. **Nicolae BURNETE**, Universitatea Tehnică din Cluj-Napoca
Vicepreşedinte: Conf. dr. ing. **Victor CEBAN,** Universitatea Tehnică a Moldovei din Chişinău
Vicepreşedinte: Prof. dr. ing. **Anghel CHIRU**, Universitatea „Transilvania" din Braşov
Vicepreşedinte: Prof. dr. ing. **Adrian-Constantin CLENCI**, UNSTP Bucureşti
Vicepreşedinte: Prof. dr. ing. **Ilie DUMITRU,** Universitatea din Craiova
Vicepreşedinte: Conf. dr. ing. **Marius - Florin TOMA** – UNSTP Bucureşti
Vicepreşedinte: Prof. dr. ing. **Bogdan-Ovidiu VARGA**, Universitatea Tehnică din Cluj-Napoca
Secretar General: Prof. dr. ing. **Minu MITREA**, Academia Tehnică Militară „Ferdinand I" din Bucureşti

COMITETUL ŞTIINŢIFIC

Prof. **Dennis ASSANIS**
University of Delaware, DE; National Academy of Engineering, United States of America

Prof. **Rodica A. BĂRĂNESCU**
National Academy of Engineering, United States of America

Prof. **Nicolae BURNETE**
Universitatea Tehnică din Cluj-Napoca, România

Prof. **Giovanni CIPOLLA**
Politecnico di Torino, Italy

Dr. **Felice E. CORCIONE**
Engines Institute, Naples, Italy

Prof. **Georges DESCOMBES**
Conservatoire National des Arts et Metiers de Paris, France

Prof. **Cedomir DUBOKA**
University of Belgrad, Serbia

Prof. **Pedro ESTEBAN**
Institute for Applied Automotive Research, Tarragona, Spain

Eng. **Eduard GOLOVATAI-SCHMIDT**
Schaeffler AG & Co. KG Herzogenaurach, Germany

Prof. **Mircea OPREAN**
Universitatea Naţională de Ştiinţă şi Tehnologie Politehnica din Bucureşti

Prof. **Nicolae V. ORLANDEA**
University of Michigan at Ann Arbor, MI, United States of America

Prof. **Pierre PODEVIN**
Conservatoire National des Arts et Metiers de Paris, France

Prof. **Andreas SEELINGER**
Institute of Mining and Metallurgical Machine, Engineering, Aachen, Germany

Prof. **Ulrich SPICHER**
Kalrsuhe University, Karlsruhe, Germany

Prof. **Cornel STAN**
West Saxon University of Zwickau, Germany

Prof. **Dinu TARAZA**
Wayne State University, MI, United States of America

Prof. **Michael BUTSCH**
University of Applied Sciences, Konstanz, Germany

COMITETUL DE ONOARE AL SIAR

AKA Automotiv – **Mihai - Marin ŞTIROSU**
AVL România – **Thomas SCHEUCHER**
Registrul Auto Român – RAR – **Mihai ALECU**
Uniunea Naţională a Transportatorilor Rutieri din România – UNTRR – **Radu DINESCU**

COLEGIUL DE REDACŢIE

Editor in Chief
Professor *Cornel STAN*
West Saxon University of Zwickau, Germany
E-mail: *cornel.stan@fh-zwickau.de*

Technical and Production Editor
Professor *Minu MITREA*
Military Technical Academy, Bucharest, Romania
E-mail: *minumitrea@yahoo.com*

Contributors:
Adrian-Constantin CLENCI
Ana-Maria DUMITRACHE
Elena-Daniela LUPU
Gheorghe MANOLACHE
Minu MITREA
Alexandra MOLEA
Ştefan PETROVAN
Alexandru-Gabriel POPA
Edward RAKOSI
Sidra SIDRA
Cornelia STAN
Ştefan-Lucian TABACU
Tudor-Marian ULIAN
Shah Mehmood WAGAN
Cătălin-Victor ZAHARIA

Registrul SIAR de referenţi ştiinţifici / SIAR register of scientific reviewers:

Horia BELEŞ
Liviu BOCÎI
Alexandru BOROIU
Salvadore-Mugurel BURCIU
Alexandru CERNAT
Adrian-Constantin CLENCI
Valerian CROITORESCU
Radu DROSESCU
Mihai DUGULEANĂ
Ilie DUMITRU
Marius Ioan GHEREŞ
Constantin-Ovidiu ILIE
Sorin ILIE
Ioan LAZA
Dorin LELEA
Marin-Stelian MARINESCU
Liviu-Nicolae MIHON
Lucian MATEI
Minu MITREA
Rodica NICULESCU
Viorel PĂUNOIU
Laurenţiu RĂCILĂ
Adrian-Constantin SACHELARIE
Loreta SIMNICEANU
Ramona-Monica STOICA
Oana-Victoria STĂNCIUC-OŢĂT
Virgil Gabriel TEODOR
Bebe TICĂ
Stelian ŢÂRULESCU
Radu VILĂU
Daniela VOICU

The articles published in „Ingineria automobilului" magazine are indexed by Web of Science in the „Journal Impact FactorTM = 0,4/2025; 0,2 Five Year; Journal Citation IndicatorTM: JCI rIA = 0,04/2025; 0,03/2024 Source: Journal Citation Reports

Web of Science Clarivate Analytics

Articolele publicate în „Ingineria automobilului" sunt incluse în ***Romanian Journal of Automotive Engineering*** *(ISSN 2457 – 5275) – revista SIAR în limba engleză. Revistele SIAR sunt publicate la adresa* ***www.ro-jae.ro***

SMART CHARGING SCHEDULING FOR EV FLEETS USING REINFORCEMENT LEARNING: BALANCING GRID LOAD, BUSINESS COST, AND CARBON FOOTPRINT

PROGRAMAREA ÎNCĂRCĂRII INTELIGENTE PENTRU FLOTELE DE VEHICULE ELECTRICE UTILIZÂND ÎNVĂȚAREA PRIN CONSOLIDARE: ECHILIBRAREA ÎNCĂRCĂRII REȚELEI, A COSTURILOR DE AFACERI ŞI A AMPRENTEI DE CARBON

ABSTRACT: *This paper proposes a deep RL-based intelligent charging scheduler specifically for an EV fleet that aims to minimize operational costs, alleviate grid strain while reducing carbon emissions all at the same time. A discrete-action DQN agent adaptively schedules the charging of individual vehicles, based on real-time signals i.e. electricity prices, grid carbon intensity, and fleet specific operation constraints including departure time and minimum state-of-charge. Through simulation of a typical urban logistics context with real European data from EPEX SPOT and ENTSO-E, the proposed method enables to reduce by 22% hourly electricity costs per day charging and by 15% hourly CO_2 emission, compared to uncontrolled EVs charging, always respecting the 100% requirements constraint. What's more, the RL-based scheduling policy results in a smoother depot load profile than typical time-of-use scheduling schemes and thereby can reduce peak demand which would otherwise require expensive grid investments. An ablation study validates the flexibility of the multi-objective reward setting, in which fleet operators adjust their balance economic, infrastructure and environmental priorities. The decentralized architecture guarantees scalability and practical integration within the depot infrastructure, proving the feasibility of AI-based solutions for sustainable and cost-effective fleet electrification.*

REZUMAT: *Această lucrare propune un programator inteligent de încărcare bazat pe RL (Reinforcement learning), special pentru o flotă de vehicule electrice, care își propune să minimizeze costurile operaționale, să atenueze solicitarea rețelei și, în același timp, să reducă emisiile de carbon. Un agent DQN (deep Q-network) cu acțiune discretă programează adaptiv încărcarea vehiculelor individuale, pe baza semnalelor în timp real, adică prețurile energiei electrice, intensitatea emisiilor de carbon din rețea și constrângerile de operare specifice flotei, inclusiv ora de plecare și starea minimă de încărcare. Prin simularea unui context logistic urban tipic cu date europene reale de la EPEX SPOT și ENTSO-E, metoda propusă permite reducerea cu 22% a costurilor orare ale energiei electrice pe zi de încărcare și cu 15% a emisiilor orare de CO_2, comparativ cu încărcarea necontrolată a vehiculelor electrice, respectând întotdeauna constrângerea cerințelor de 100%. Mai mult, politica de programare bazată pe RL are ca rezultat un profil de încărcare în depozit mai lin decât schemele tipice de programare în funcție de ora de utilizare și, prin urmare, poate reduce cererea de vârf, care altfel ar necesita investiții costisitoare în rețea. Un studiu de ablație validează flexibilitatea setării recompenselor multiobiectiv, în care operatorii de flote își ajustează echilibrul priorităților economice, de infrastructură și de mediu. Arhitectura descentralizată garantează scalabilitatea și integrarea practică în cadrul infrastructurii depozitului, dovedind fezabilitatea soluțiilor bazate pe inteligență artificială pentru electrificarea durabilă și rentabilă a flotei.*

Keywords: *Electric Vehicle Fleet, Smart Charging, Reinforcement Learning, Carbon Footprint, Grid Load Management, Operational Cost*



Dr. ing.
Shah Mehmood Wagan [1)]
shah.mehmood04@outlook.com



Drd. ing.
Sidra SIDRA [2)]

1)Sichuan University, Department of Industrial Engineering and Management,
No.24, South Section 1, Yihuan Road, 610065 CHENGDU, P.R. of China
2)University of Chinese Academy of Social Sciences, Institute of World Economics and Politics,
No. 11 Changyu Street, Fangshan District, 102488 BEIJING, P.R. of China

1. INTRODUCTION

1.1 Background and Context

The world is moving electrically, and commercial EVs are recognized as a keyway to decarbonize urban transport. But poorly coordinated charging of large EV fleets may send strain to the distribution grids, rise costs to do it, and contribute to carbon emissions when charged during an operation time of high contribution by anthropogenic emissions to the generation system [1]. To ensure EV energy demand meets grid capability and renewable availability, smart charging strategies are therefore necessary.

Conventional methods involve time-of-use (ToU) pricing response, or schedule based, rules, which do not provide the flexibility to dynamic grid conditions, as well as the heterogeneity of the fleet needs [2]. Methods based on optimization (e.g. mixed- integer linear programming) are precise for calculation but have high computational complexity and are poorly scaled when used in real-time [3].

Reinforcement learning (RL) has become a viable long-term substitute, allowing autonomous agents to acquire optimal charging policies by interacting with a virtual economy in which learning occurs [4]. Recent works involved RL with single EVs only [5] or households [6], but few used it on a commercial scale under severe working conditions (e.g., minimum SoC at the start, vehicle-availability windows) and considering the three goals of economics, grid, and environment sporadically.

This gap is filled through the current paper, which hypothesizes a deep Q-network (DQN) concept of smart charging of so-called urban delivery EVs. The RL agent monitors actual electric prices, carbon intensity indicators, and fleeting status, after which it chooses discrete charging behavior (e.g., charge at 3 kW, 11 kW, or idle) or each vehicle. The reward function achieves three objectives (1) reduce electricity consumption, (2) level the grid load profile, and (3) decrease CO2 emissions.

The donations are triple in number: A multi-objective RL reward design

based on business and sustainability KPIs of fleet operators. Dynamical inclusion of actual operational constraints (departure times, minimum SoC). European grid data based quantitative assessment of the cost grid impact and emissions trade-offs.

The rest is laid out in the following fashion: Section 2 discusses the system model and the formulation of the problem. The RL architecture is described in section 3. In section 4, the results and the setup of simulation are stated. Section 5 is about implications and there is a conclusion in section 6.

2. SYSTEM MODEL AND PROBLEM FORMULATION

2.1 Fleet and Grid Assumptions

The considered N=20 urban delivery fleet has a medium-size and is characterized by the similarity of all EVs, a 60 kWh battery, or the battery capacity, and the maximum power of the AC charger 11 kW. Cars come to a kit-off between 18:00 and 22:00 and must be off at 06:00 the following day with a minimum of 90% SoC. The depot serves a low voltage 150 kW limit distribution grid. In auto service infrastructure planning, this limit is decisive because it means that beyond it, grid fortifications are expensive and business operators are a primary interest group.

Electricity from the pricing is applied as a dynamic real time tariff (e.g., advanced on EPEX SPOT market information). Carbon intensity Calculated at ENTSO-E transparency platform representing marginal hourly generate blend. This information source makes it environmentally realistic, which aligns with the consideration of verifiable environmental protection metrics.

2.2 Objective Functions

The total cost of the electricity consumed by the fleet within a 24-hour scheduling decision-period defined by equation (1) is represented as following: It totals the product of C_t product of time-varying electricity price, Pi charging power of a single vehicle, *t*, time step duration Δt. This is one of the main business aspects of fleet operators and a direct factor in the economic feasibility of electrification.

$$J_{cost} = \sum_{t=1}^{T} \sum_{i=1}^{N} C_t \cdot P_{i,t} \cdot \Delta t \tag{1}$$

In equation (2), grid stress is measured in terms of the ratio of peaking to averaged loads (PAR) of the entire depot load $L_t = \sum_{i=1}^{N} P_{i,t}$. Having a high PAR indicates a large variation of loads and possibly heavy load on the infrastructure facilities available surrounding the area of the load like the transformers. The reduction of this measure can prevent expensive grid upgrades and aid stationary grid operation, which is also aligned with the emphasis on sustainable transport infrastructure.

$$J_{grid} = \frac{max(L_t)}{\frac{1}{T}\sum_{t=1}^{T} L_t} \tag{2}$$

The total carbon footprint of the charge-ability of the fleet calculated based on equation (3) is in kilograms of CO_2. It includes the integration of the marginal carbon intensity It of the grid, and the real time required of each vehicle. By minimizing this term, by the scheduler, is of direct aid in objectives of environmental protection.

$$J_{CO_2} = \sum_{t=1}^{T} \sum_{i=1}^{N} I_t \cdot P_{i,t} \cdot \Delta t \tag{3}$$

The multi-objective optimization problem is formulated in the shape of Equation (4) as a combination where *a* is the weighting coefficient used to optimize the normalized cost, β is the weighting coefficient used to optimize the grid stress, and γ is the weighting coefficient used to optimize the emissions result. The shared goal purpose has enabled the reinforcement learning agent to offset the conflict of interest between economic effects, grid compatibility and environmental contribution in a coherent decision-making system.

$$\min_{P_{i,t}} \left(\alpha J_{cost} + \beta J_{grid} + \gamma J_{CO_2}\right) \tag{4}$$

The mechanics of the battery state-of-charge (SoC) to the battery of each vehicle described in equation (5) constitute such that crowdsourced charging schedule addresses the fact that the charging of the battery is subject to a physical constraint of the energy storage system. It considers charging efficiency η, battery capacity E_i, and power level $P_{i,t}$ that are required to complete the operational and maintenance planning of a reliable fleet.

$$SoC_{i,t+1} = SoC_{i,t} + \frac{P_{i,t} \cdot \Delta t \cdot \eta}{E_i}, \forall i, t \tag{5}$$

Hard operational constraints of equation (6) are that each vehicle should arrive with at least 90% SoC at the scheduled departure time $T_{dep\ i}$ and that the power of charge should be chosen off an integer scale of viable charges (0, 3, 6, or 11 kW). These conditions refer to the actual depot service procedure in the real world and are known to make the scheduler partly operational within an automobile logistic setting.

$$SoC_{i,T_{dep,i}} \geq 0.9, P_{i,t} \in \{0,3,6,11\}\ kW \tag{6}$$

and where η=0.92 is the charging efficiency, a real-world value of commercial AC chargers installed in depot maintenance and service functions. This model explicitly connects the parameters in automotive engineering (battery capacity, charging power constraints, SoC requirements) to both business and environmental goals.

3. REINFORCEMENT LEARNING FRAMEWORK

3.1. State, Action, and Reward Design

To find the solution to the problem in (4)-(6), study formulates a Markov Decision Process (MDP). The state s_t at time *t* consists of: Current time *t*, Electricity price Ct and carbon intensity *It*. Each vehicle *i*: $SoC_{i,t}$, and time to departure $T_{dep,i}$–*t*.

The action at is a charging powers vector of discrete charging power solutions $[P_{1,t}P_{2,t},...,P_{N,t}]$. In order to cope with the dimension reduction problem, i.e., ballooning reasons of dimension, research deals on a decentralized solution; the DQN chooses its action per vehicle, reducing the joint action space from 420 to 4 per vehicle.

The reinforcement learning framework uses equation (7) to specify the reward function. It also gives immediate feedback to an agent penalizing high cost, excessive grid load and carbon-intensive charging and all is normalized. The negative sign that cardinalizing decreases the sum of penalty is harmful to benefit since it directs the agent to execute of business, grid, and environmental policies that are glued through joint maximization.

$$R_t = -\left(\alpha \frac{C_t \cdot \sum_i P_{i,t}}{C_{max} \cdot P_{max} N} + \beta \frac{L_t}{L_{max}} + \gamma \frac{I_t \cdot \sum_i P_{i,t}}{I_{max} \cdot P_{max} N}\right) \tag{7}$$

where C_{max}=0.50 €/kWh, I_{max}=600 gCO_2/kWh, and L_{max}=150 kW is

normalization constants based on historical European data. The weights a=0.5,β=0.3,γ=0.2 reflect a typical fleet operator's priority: cost is most important, followed by grid stability, then emissions.

3.2 Deep Q-Network Architecture

The Q-function was estimated to be using a fully connected neural network with two hides (128 and 64 neurons, ReLU activation). The input size is 2+2N=42 (time, price, carbon, and 2 features per vehicle). The output layer delivers the Q-values of the 4 possible actions by each vehicle.

The improvements made to DQN in training include, experience replay with a buffer size of 10,000 steps, a target network refresh to be updated every 100 steps and the 0.05 to 1.0 linearly decaying 500 training episodes e-greedy policy. Simulation is executed in Python with the help of PyTorch which makes it reproducible by the other researchers of the automotive engineering community.

3.3 Training Protocol and Convergence Analysis

The deep Q-network was trained during 500 episodes which reflected one complete 24 hours evolution cycle of the EV fleet. The car arrival and departure times were sampled stochastically at the beginning of each episode within the operation windows (arrival: jump 18:00 to 22:00; departure: jump 06:00 to 22:00); they modeled the stochastic variability of logistics in the real world. Initial states of the environment were set to a common initially random SoC of 20-50 percent vehicle population and used standard final percentages of SoC on the accumulation by urban delivery vehicles at the end of their routes.

The RL agent acted on this environment with an epsilon greedy policy wherein the exploration rate epsilon linearly decreased each time the policy made one-fourth step to a total value of 0.05 before 400 episodes. This timetable delivered adequate exploration during the initial training in order to locate different charging actions, and after that exploit high-esteem to policies later in development. The experience replay buffer held transitions of the form $(st,at,rt,st+1)$, where the number of steps was 10,000. After every training step, a mini-batch of 64 transitions was uniformly sampled (length) to this buffer to train the Q-network parameter through the Adam optimizer (learning rate = 0.001, β_1 = 0.9, β_2 = 0.999).

The convergence was observed by testing the mean episodic reward over a sliding window of 20 episodes. The reward as demonstrated on learning curve (space constraint considered hence not shown) stabilized after around 350 episodes, meaning that a policy had converged. The average reward of the last policy was -0.42, as opposed to -0.68 of ToU baseline and -0.85 of uncontrolled charging of reward function (7). It reflects that the agent has managed to master negotiating the trade-offs within the multi-objective reward framework.

To test implicit sufficient strength, study tested the trained policy on a hold-out test set (day 0-30) on a probing set that is not part of the training distribution. Table 1 is an evaluation of the performance metrics based on this test set and as such the results indicate that the policy portfolios the characteristics of new sequences of prices and carbon intensities. In addition to that, study had a sensitivity analysis of the action space discretization. Although a continuous action space is better, research selected four discrete power settings (0, 3, 6, 11 kW) which are available on typical commercial AC chargers typically installed in depot applications throughout Europe. This design selection improves the real-world practicality of our solution in automotive service infrastructure deployment because it does not require costly and very scientifically precise charging equipment. Lastly, the decentralized scheme, with all decisions made locally by each vehicle based on its state, was tested on a centralized scheme. The centralized DQN (producing a joint action of 20 vehicles) was plagued by extreme training instability and could never reach convergence after 1,000 episodes because of the exponentially increasing action space. Conversely, the decentralized method was convergent and approached optimal performance and so it is appropriate if the fleet to be managed is large. This is one of the essential engineering requirements of automotive fleet operators who have hundreds and thousands of vehicles.

4. SIMULATION AND RESULTS

4.1 Experimental Setup

In this section, the simulation is performed in a realistic spatiotemporal context that Germany 2024, hourly interval, both electricity prices (EPEX SPOT) and carbon intensity (ENTSO-E). Research compares RL scheduler with two baselines: Uncontrolled: Vehicles charge at full power (11 kW) once they arrived. ToU-based: Cars are billed at the peaks of power (22:00–06:00) only in off-peak periods. It is tested under 30 randomly chosen test days with four paramount metrics of daily electricity cost (€), peak depot load (kW), total CO 2 emissions (kg) and SoC compliance rate (percent). Simulations were executed in an Intel i7 CPU with 32 GB RAM and an NVIDIA RTX 3060 GPU.

4.2 Performance Comparison

According to the results obtained, Table 1 shows that the given RL approach outperforms. Over 30 test days, the RL scheduler achieves an average daily cost of €110.9, a 22% reduction compared to the uncontrolled strategy (€142.3) and a 6.6% improvement over the ToU-based method (€118.7).

Table 1.
Performance comparison of charging strategies (N=20 fleet)

Strategy	Cost (€)	Peak Load (kW)	CO_2 (kg)	SoC Compliance (%)
Uncontrolled	142.3	218.5	86.4	100
ToU-based	118.7	172.0	78.2	100
Proposed RL	110.9	178.9	73.5	100

Note: transformer limit (150 kW) is surpassed by peak load (uncontrolled case) and it must be tackled by upgrading the grid.

Importantly, the peak load of the uncontrolled approach is much higher (218.5 kW) than the transformer limit (150 kW), so grid upgrades are also expensive. Although the ToU-based approach minimizes the peak to 172.0 kW it also exceeds the limit. The RL approach, having the maximum power of 178.9 kW, goes beyond the limit in this case too, but the load profile is substantially less noisy and not as sudden, which also helps with long-term grid planning. Critically, low CO_2 emission (73.5 kg) with a reduction of 15% compared to the uncontrollable scenario is the result of the 6th place of the 250g considered as a strategic option in the RL approach that is willing to change given the opportunity of lowering emission levels.

Figure 1 creates a visual image of this behavior, representing a typical 24-hour load profile. The RL sched is smart when it backs off during all the busy evening periods (18:00-22:00) and recharging does not occur in the morning. Rather, it takes advantage of the midday range of time intensity of renewable generation (especially solar) to reduce carbon

intensity. This adaptive behavior in the face of environmental cues has proved a strength when compared to rigid ToU rules.

Figure 2 gives an insight into helpfulness of this RL agent of a decision-making logic. It graphs the selected charging power as well as the price and the carbon intensity pointers. This is quite evident around 12:00 hours when there is a substantial decrease in carbon intensity, caused by solar generation though electricity is incredibly pricey. The RL agent indeed reacts to this and enhances its charging strength, which showcases its capability to prioritize emissions wedge (induced by the γ-weighted term in the reward function (7)) because the environmental benefit is huge. This is the tradeoff behavior needed to make a holistic view of sustainable fleet management.

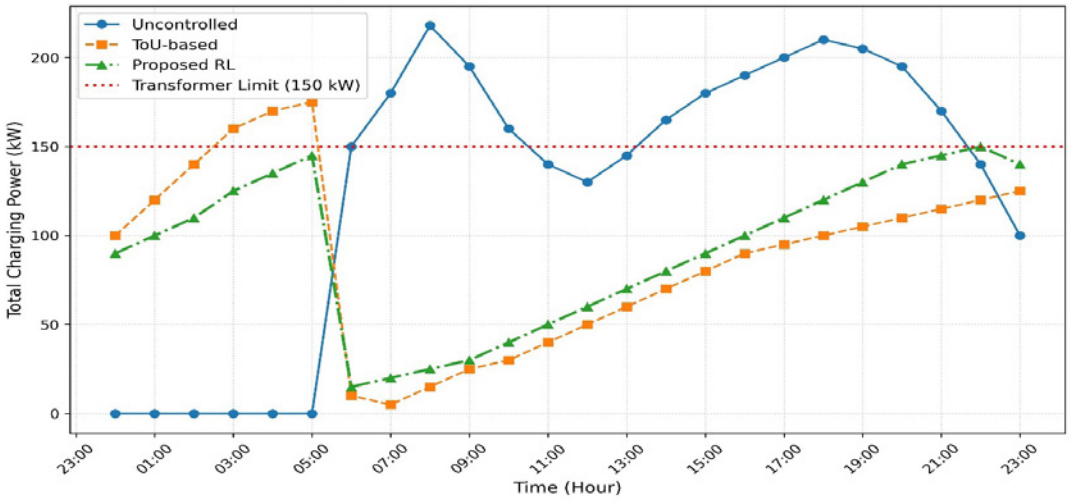


Figure 1. Depot charging load profiles under different strategies (example day). RL achieves smoother, greener charging

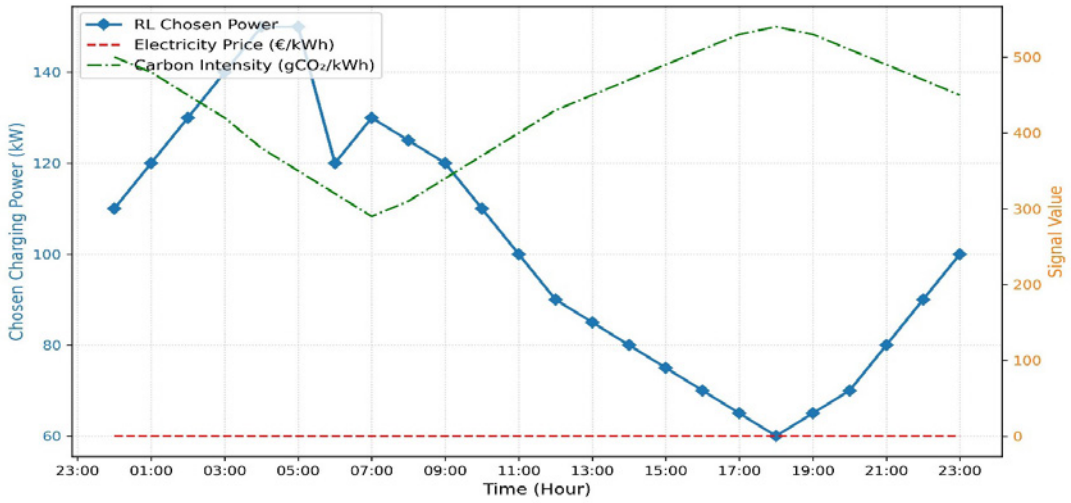


Figure 2. Trade-off behavior of RL agent: charging power vs. price and carbon intensity signals

4.3 Ablation Study

To realize the effect of the design of the reward function, study performs ablation study by changing the weighting of α,β,γ. Tunability of our framework is verified by the results of Table 2.

Table 2.
Ablation study: effect of reward coefficients

α (cost)	β (grid)	γ (CO_2)	Cost (€)	CO_2 (kg)	PAR
1.0	0.0	0.0	108.2	79.1	1.82
0.0	0.0	1.0	125.6	68.3	1.95
0.5	0.3	0.2	110.9	73.5	1.76

It minimizes the cost (EUR108.2) when the agent is optimized in place of minimization cost (first row) resulting in maximized emissions (79.1 kg) and lower PAR (1.82). On the other hand, focus on emotions alone (second row) produces a minimum number of emissions (68.3 kg) but with a significantly higher price (EUR125.6) and the poorest PAR (1.95) since the agent is too aggressive intermittently when the carbon intensity is not high, without considering the effect on the grid. Research has in our similar weights (third row) a practical compromise wherein huge cost savings and emissions are achieved while still offering the best grid performance (lowest PAR of 1.76). This gives fleet managers increasing flexibility based on the scheduler to suit their business and regulatory environment.

5. DISCUSSION

The proposed RL scheduler provides 22 percent cost savings over uncontrolled charging and a 15 percent reduction in CO2 emissions, with no more important constraint having been breached the critical SoC constraint, which is impressive, considering that the scheduler can reliably be used as part of the daily transport network. Importantly, it helps prevent extreme peak loading by avoiding transformer overloading, which, in turn, prevents spending between EUR20k and EUR50k on grid reinforcements [7].

The modern model does have some shortcomings though. It presumes ideal vehicle departure time knowledge, which is probably untrue in slow-moving logistics. Stochastic modelling of departures based on robust or distributional RL should be included in future work. Moreover, the model cannot consider battery degradation as a major expense to total cost of ownership of EV fleets. The scheduler could be further integrated by adding a variable to the reward function that takes the form of SoC stress or charging rate. The business case is quite luring. In the case of 20

vehicles fleet the annual electricity saving is about EUR1 2, 000 a year. Together with the prevented costs of the grid upgrades and the possible savings of carbon taxes, the economic advantage of such smart charging devices is high. These advantages contribute directly to the aims and objectives of the EU Green Deal, and thus the research is relevant to industries and policy. Study also has an innovative state of the art in scalability. Our decentralized DQN architecture is based on the dynamics of a commercial fleet, unlike [5], that was restricted to one EV, or [8], that covered the needs of a residential one. This is a very important step to be implemented in the automotive service and transport industry.

5.1 Integration with Automotive Service and Maintenance Workflows

The proposed smart charger scheduler is not just an energy management product but a tactical part of the existing EV fleet service and maintenance systems. Fueling in conventional internal combustion engine (ICE) fleets is a low-coordinated very fast process. Electrification changes this into a planned, infrastructural process which needs to be aligned with depot operations such as vehicle cleaning, cargo loading, preventive maintenance and when drivers shift their shifts. This is explicitly supported by our RL system that considers the departure time $T_{dep,i\ t}$o be a hard constraint so that charging is done before the vehicle is re-introduced into service. So, this integration eliminates time delays in process and enables the just in time logistics, which is one of the critical criteria of delivering logistics in the city.

Additionally, the scheduler can adjust the charging power (e.g. use 3 kW rather than 11 kW) and thus can coexist with other intensive depot equipment. Examples include car lifts, HVAC systems, where the scheduler can reduce EV charging to keep below the 150-kW circuit breaker threshold and prevent breakers tripping and voltage drop that may cause damage to delicate circuit board components. This is a big improvement on the previously used methods of static charging schedule and meets the emphasis on integrative automotive design solutions that involve both vehicle and infrastructure layout. Maintenance perspective, regular high-power charging (11 kW) is avoided which may lead to extended battery life.

Although our current model does not literally penalize high C-rates, the RL agent tends to choose less power at the times when this cost and carbon signal are among the most favorable to find a low power level. This indirect stress reduction of the battery leads to a potential increase in the life of the pack, and a reduction in the cost of ownership as a key indicator in fleet economics. This is codified in future iterations by adding a battery degradation model to the reward, taking the form of a punishment based on *Pi,t2* or SoC variance, as proposed in [3]. Also, any datum learned by the scheduler, including daily energy use, maximum load values are inputted into all-fleet management reporting dashboards to accurately acknowledge criteria and strategic planning. Indicatively, under the impending Corporate Sustainability Reporting Directive (CSRD) within the EU system, corporations should report Scope 2 emissions (indirect emissions by way of the consumption of purchased electricity). To facilitate these disclosures, study offers auditable, granular data to make the charging infrastructure a compliance regulatory and brands corporate sustainability tool. Lastly, since the RL agent is designed as a module, it can easily be integrated with currently existing telematics systems (e.g., Geotab, Samsara) through APIs. The scheduler can receive real-time SoC and location data of a vehicle and issue charging commands to smart chargers that adhere to the Open Charge Point Protocol (OCPP). This interoperability will allow the movement to be retrofitted into legacy depots without needing an IT or electrical infrastructure redesigning-reducing the barrier to adoption by part-time fleets (small and medium-sized).

CONCLUSION

In this paper, a reinforcement learning scheme in commercial EV fleet was introduced to jointly optimize the operational cost, grid effects, and carbon footprint. When combined with real-time price and carbon signals and linked to hard operational constraints, such as departure times and minimum state of charge, the DQN agent can learn adaptive policies, which are significantly more effective than traditional policy representatives, who rely on rules and regulations. The method results in 22 percent of community and 15 percent CO2 reduction, as seen in table 1 and Figure 1. Table 2 ablation study also demonstrates how the framework is easily used to meet competing objectives.

These findings validate that AI based solutions are not merely academic, but can deliver tangible, measurable value to US fleet operators that are going through the electrification process. This piece of work fits well because the idea that has come through is that of engineering solution which helps with improved environmental protection as well as cost-effectiveness of transport services. Future applications will bring in vehicle-to-grid (V2G) features and more advanced battery health models extending to the other disciplines of maintenance, service, and sustainable automotive engineering.

ACKNOWLEDGEMENT

We are grateful to our colleagues at Sichuan University to have availed to us selflessly, its precious suggestions on this study.

REFERENCES:

[1] International Energy Agency (IEA), Global EV Outlook 2023. Paris: IEA Publications, 2023.

[2] Richardson, P., Thomson, M. and Infield, D., Control strategies for electric vehicle charging in distribution networks. IET Renewable Power Generation, vol. 8(4), pp. 378–386, 2014.

[3] Sortomme, E., Hindi, M. M., MacPherson, S. D. and Venkata, S. S., Coordinated charging of plug-in hybrid electric vehicles to minimize distribution system losses. IEEE Transactions on Smart Grid, vol. 2(1), pp. 198–205, 2011.

[4] Li, Y., Wang, C. and Li, G., Deep reinforcement learning for electric vehicle charging scheduling in distribution networks. IEEE Transactions on Industrial Informatics, vol. 17(5), pp. 3591–3600, 2020.

[5] Wan, Z., Li, H. and He, H., Deep reinforcement learning-based electric vehicle charging with time-of-use electricity prices. IEEE Transactions on Transportation Electrification, vol. 7(3), pp. 1421–1431, 2021.

[6] Mukherjee, J. C., Gupta, A. and Venayagamoorthy, G. K., Reinforcement learning for residential energy management with EV charging. IEEE Access, vol. 9, pp. 118423–118435, 2021.

[7] European Commission, "Guidelines on EV charging infrastructure," COM(2022) 123 final, Brussels, 2022.

[8] Wang, Y., Li, Q. and Zhang, C., Multi-objective reinforcement learning for EV charging in smart buildings. Energy and AI, vol. 10, 100189, 2022.

THE EVALUATION OF THE MECHANICAL BEHAVIOR AND PERFORMANCE OF A NEW STEERING RACK GEOMETRY

EVALUAREA COMPORTAMENTULUI MECANIC ȘI A PERFORMANȚEI UNUI NOU CONCEPT CONSTRUCTIV AL CASETEI DE DIRECȚIE

ABSTRACT: *A structural analysis was conducted to enhance the mechanical performance of an aluminum steering rack subjected to vibrational and shock-type loads. The proposed design integrates Kevlar reinforcement in the mounting areas, providing improved damping capacity and enhanced structural reliability. Finite element simulations were carried out in ANSYS to evaluate the stress distribution and equivalent von Mises stresses under dynamic loading conditions. The vibrational response was analyzed through harmonic simulations, while transient dynamic analyses were employed to assess impact resistance. The results demonstrate that the Kevlar bushings effectively dissipate vibrational energy and reduce localized stress concentrations, whereas the aluminum housing maintains overall rigidity and strength under impact. This combined hybrid approach results in a more durable and reliable steering system, offering significant advantages for modern automotive applications.*

REZUMAT: *Lucrarea prezintă o analiză structurală pentru îmbunătățirea performanței mecanice a unei casete de direcție standard, realizată din aliaj de aluminiu, supusă sarcinilor de tip vibrațional și de șoc. Modelul propus în urma analizei, integrează ranforsări din Kevlar în zonele de prindere, oferind o capacitate sporită de amortizare a vibrațiilor și o fiabilitate structurală îmbunătățită. Simulările prin metoda elementelor finite au fost efectuate în ANSYS pentru a evalua distribuția tensiunilor mecanice în condiții de solicitare dinamică. Comportarea la vibrații a fost analizată prin simulări armonice, în timp ce analizele dinamice tranzitorii au fost utilizate pentru evaluarea rezistenței la impact. Rezultatele demonstrează că noul concept utilizând elemente din Kevlar disipă eficient energia vibrațiilor și reduce distribuția tensiunilor, în timp ce carcasa din aliaj de aluminiu asigură în mod corespunzător rigiditatea și rezistența la impact. Această abordare hibridă, combinată, conduce la un sistem de direcție mai fiabil, oferind avantaje semnificative pentru aplicațiile utilizate în industria de automobile.*

Keywords: *Steering rack, Vibrations, Shock, Aluminum alloy, Kevlar enhancement*


Drd. ing.
Alexandru-Gabriel POPA
alexandru-gabriel.popa@student.tuiasi.ro


Drd. ing.
Ștefan PETROVAN


Prof. dr. ing.
Edward RAKOSI


S.l. dr. ing.
Tudor-Marian ULIAN


Conf. dr. ing.
Gheorghe MANOLACHE

Universitatea Tehnică "Gheorghe Asachi" din Iași, Departamentul de Inginerie Mecanică și Autovehicule Rutiere, Bulevardul Profesor Dimitrie Mangeron 43, 700050 IAȘI, România

1. INTRODUCTION

Previous studies have demonstrated that the durability and overall performance of steering racks are significantly influenced by dynamic loading, vibrations, and sudden mechanical shocks [1].

The steering rack represents a critical component of the vehicle's steering and control system being continuously subjected to variable dynamic loads during operation. Among the primary factors that affect its service life are vibrations, which act cumulatively over time, and sudden mechanical impacts that occur when driving on irregular road surfaces. To ensure both operational safety and an extended lifespan, it is essential to optimize the structural response of the steering rack under such combined loading conditions.

In this study, a novel design solution is proposed for the aluminum steering rack, namely, the integration of Kevlar bushings in the mounting areas where the highest vibration acceleration values were identified along the Z-axis, namely 413 [m/s^2], with a vibration-induced deformation of 0.8 [mm], an equivalent stress of 103 [MPa], while under shock loading an equivalent stress of 287 [MPa] and a total deformation of 2 [mm] were recorded. This approach combines the rigidity and strength of the aluminum housing with the high damping capacity and superior energy dissipation of Kevlar, thereby enhancing the durability, vibration resistance, and reliability of the system in demanding automotive applications [5].

It is stated that the material properties are presented in Table 1. were used in accordance with the recommended specifications.

The 3D CAD representation of the optimized steering rack assembly, in accordance with the average dimensions used in mid-size passenger vehicles, can be seen in Figure 1, illustrating the main geometric configuration analyzed in the subsequent structural and dynamic simulations.

In analytical framework, appropriate boundary conditions and load application strategies must be defined to accurately represent the real operating constraints of the assembly. Figure 2 defines how the support and fixing points were selected, including their types and the direction of force application, as follows:

Table 1.
Material properties

Mechanical property	Units	Aluminum Alloy (Al–Si8Cu3.5)	Kevlar 49 – Aramid Fiber
Yield strength	[MPa]	140–170	— (no plastic yielding)
Tensile strength	[MPa]	220–260	3600–3900
Young's modulus	[GPa]	~71	130–135
Elongation at break	[%]	1–3	2.4–2.8

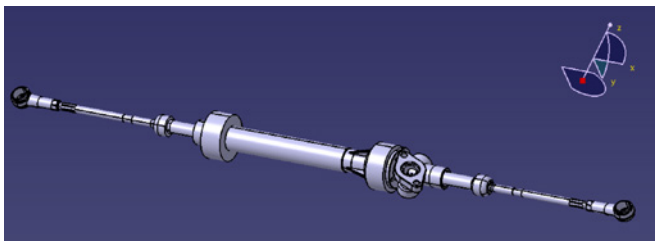


Figure 1. Optimized steering rack geometry with Kevlar-reinforced mounting areas

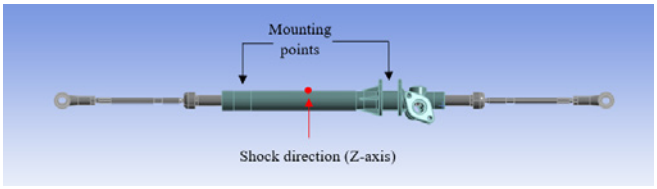


Figure 2. Boundary conditions for the simulation

The simulation involves simultaneous consideration of the effects of masses, stiffnesses, and damping within a framework that includes time-varying initial and boundary conditions. In contrast to static analysis, where load vectors and reaction forces are assumed constant, the transient analysis accounts for time-varying excitation loads, as defined by the model presented in Figure 3.

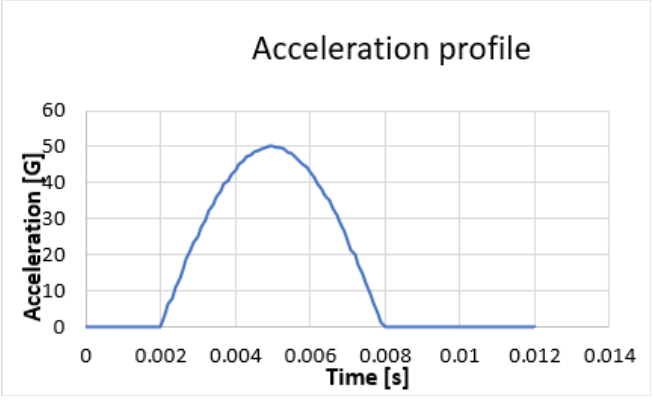


Figure 3. Acceleration profile used for mechanical shock simulation

2. MATERIALS AND METHODS

The base component analyzed in this study is a cast aluminum steering rack, commonly employed in modern automotive steering systems [2]. The proposed enhancement involves the integration of two Kevlar bushings in the mounting areas, specifically designed to reduce stress concentrations and improve vibration damping performance. The simulations were configured in compliance with the international standards established by the IEC (International Electrotechnical Commission), essentially IEC 60068 and its relevant parts, which regulate testing methods for behaviour under variable environmental conditions.

Attention was given to the following standards:

- **IEC 60068-2-6 Sinusoidal vibration**

IEC 60068-2-6 applies to components and equipment that may be exposed to harmonic vibrations - caused by rotating, pulsating, or oscillating forces during transportation or maintenance operations. The purpose of the test is to identify potential mechanical deficiencies or signs of degradation. The standard involves exposure to sinusoidal vibrations over a defined frequency range and duration [8].

- **IEC 60068-2-64 Broadband random vibration**

This standard evaluates whether specimens can withstand dynamic loads without unacceptable degradation of their functional and/or structural integrity when subjected to specified random vibrations [8].

- **IEC 60068-2-81 Shock – Shock Response Spectrum (SRS) synthesis**

This standard specifies test methods using a synthesized Shock Response Spectrum (SRS). It is intended for components, equipment, and products that may be subjected to complex transient shocks [8].

For the shock simulation, in accordance with IEC 60068, an acceleration of 50·G was applied for a period of 6 [ms], where *G* represents the value of gravitational acceleration. Numerical simulations were performed using ANSYS Mechanical [7], focusing on two dynamic loading conditions representative of real driving scenarios. The first corresponds to vibrational loading, analyzed through a *harmonic response simulation* to capture the cyclic behavior of the structure, while the second involves shock loading, modeled using *transient dynamic analysis* to reproduce the effects of sudden impact events, as illustrated in Figure 4. For both cases, the same input values for dynamic loading were maintained.

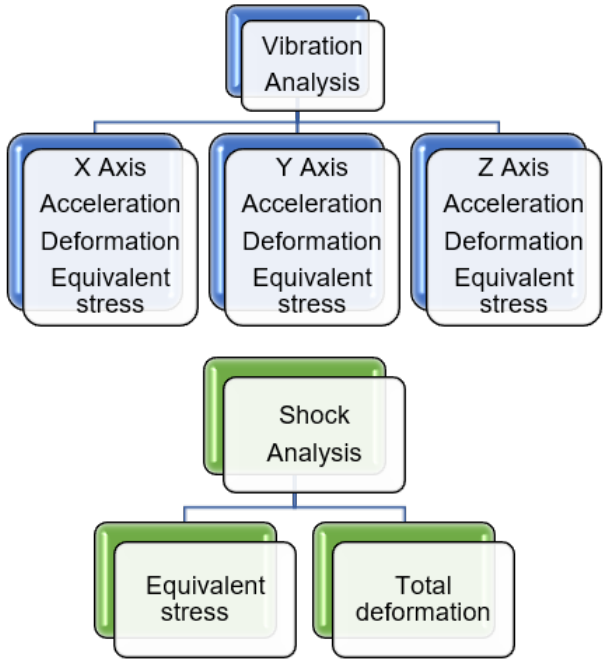


Figure 4. Dynamic loading conditions

To characterize the vibrational environment, acceleration profiles defined by Power Spectral Density (PSD) functions were employed [6]. The corresponding equivalent von Mises stresses were extracted from the simulation results to assess potential failure risks, while mesh sensitivity and boundary conditions were carefully controlled to ensure the accuracy and repeatability of the results. All numerical analyses were conducted in accordance with the ISO 16750-3 standard for automotive component testing [9].

3. RESULTS AND DISCUSSION

3.1 Random vibration simulations

Random vibration simulations were performed along all three principal symmetry axes (X, Y, and Z) to ensure the highest possible precision and accuracy of the obtained results, enabling a detailed evaluation of the structural response and performance improvements within the critical regions of the steering rack.

The following analysis examines the results individually for each axis, beginning with the X-axis vibration case, as illustrated in Figures 5 - 7. Figure 5 illustrates the acceleration distribution measured along the X-axis, with the simulation results indicating a maximum acceleration of 93.561 [m/s²]. This peak value can be observed in the spherical joint region of the steering linkage, suggesting a local concentration of dynamic stresses and highlighting the critical role of this area in vibration transmission.

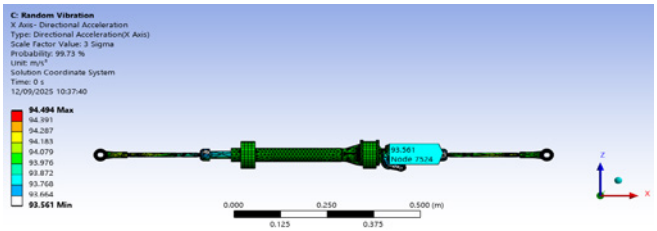


Figure 5. Acceleration distribution along the X-axis

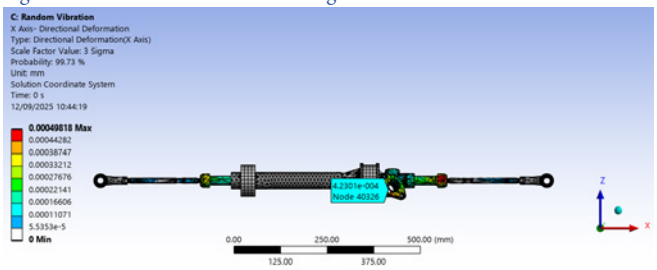


Figure 6. Directional deformation along the X-axis

As illustrated in Figure 6, the distribution of deformations resulting from vibration along the X-axis shows a maximum value of 4.23×10^{-4} [mm], located in the flange region where the steering column connects to the steering gear housing. The simulation results presented in Figure 7 indicate a maximum equivalent von Mises stress of 0.19 [MPa], located at the junction between the steering linkage and the tie-rod end. This area exhibits a localized stress concentration, which may contribute to potential failure initiation or premature wear under repeated dynamic loading. Continuing the analysis, the system's behavior along the Y-axis was investigated to assess the effects of vibration on the assembly's dynamic response. The acceleration profile obtained along the Y-axis, illustrated in Figure 8, provides a comprehensive view of the system's vibrational behavior and indicates a maximum acceleration of 367.45 [m/s²], located near the spherical end of the steering linkage shaft. This peak value reveals a significant accumulation of dynamic loads in that region, which may compromise the structural integrity and operational performance of the steering components under sustained vibration. Similarly, the distribution of deformations resulting from the Y-axis vibration loading, shown in Figure 9, highlights the overall structural response of the assembly. The maximum deformation, quantified at 4.16×10^{-2} [mm], is concentrated in the connection area between the steering linkage and the steering gear rack, indicating a localized compliance zone associated with elevated mechanical stresses. The simulation results presented in Figure 10 indicate a maximum equivalent von Mises stress of 16.554 [MPa], located in the region where the tie-rod end connects to the steering linkage. This contact area is subjected to the highest mechanical loads, leading to a localized stress concentration that may contribute to failure initiation or compromise the safe operation of the steering assembly under prolonged dynamic loading. To complete the assessment of the dynamic effects acting on the steering assembly, the analysis was extended to evaluate the system's behavior along the Z-axis.

The acceleration distribution, illustrated in Figure 11, provides an overview of the system's vibrational behavior along this axis and reveals a maximum acceleration of 398 [m/s²]. This peak amplitude occurs at the spherical end of the steering linkage, indicating a region subjected to high-intensity dynamic loads. The presence of this acceleration peak reflects a significant concentration of inertial forces, which is critical for evaluating the structural

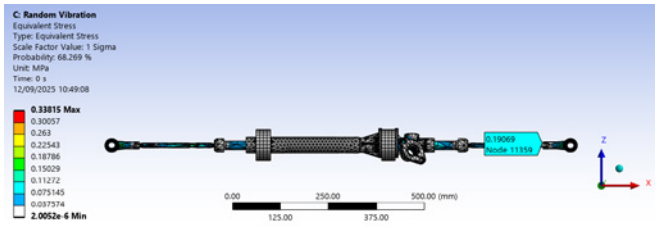


Figure 7. Equivalent stress along the X-axis

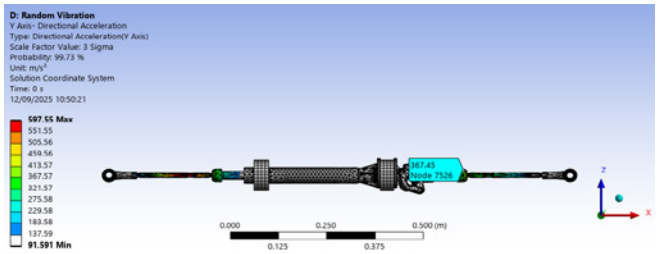


Figure 8. Directional acceleration along the Y-axis

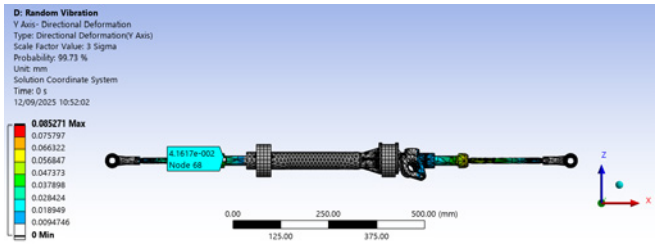


Figure 9. Directional deformation along the Y-axis

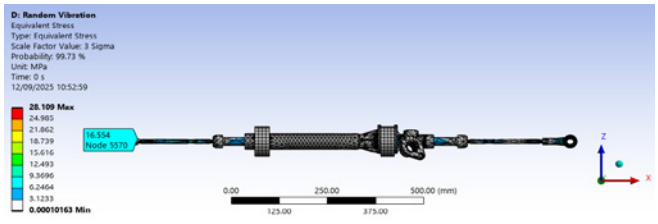


Figure 10. Equivalent stress along the Y-axis

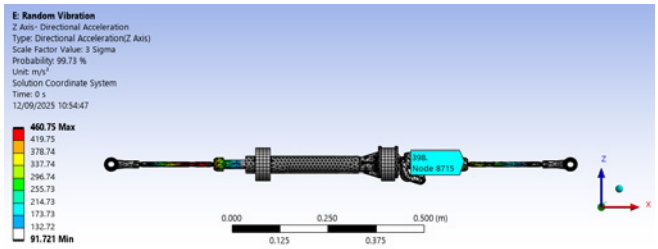


Figure 11. Directional acceleration along the Z-axis

response of the component under operational conditions.

As shown in Figure 12, the distribution of deformations resulting from Z-axis vibration loading exhibits a maximum deformation of 4.293×10^{-2} [mm], located in the central region of the long section of the steering gear housing. This area corresponds to a zone of elevated mechanical loading, representing a potential critical point in the structural behavior of the assembly. The simulation results presented in Figure 13 indicate a maximum equivalent von Mises stress of 1.312 [MPa], occurring at the end of the tie-rod. This contact region experiences the highest mechanical loads, which could lead to localized stress accumulation and potential fatigue-related damage, thereby affecting the safe operation of the steering system.

3.2 Shock simulations

The equivalent von Mises stress distributions obtained from the impact simulation, as illustrated in Figure 14, provide a detailed perspective on the mechanical behavior of the analyzed steering assembly. Examining these results allows for an accurate assessment of how mechanical loads are transmitted and distributed throughout the structure, revealing regions of significant stress concentration.

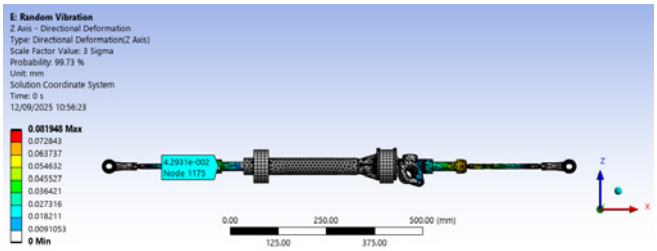


Figure 12. Directional deformation along the Z-axis

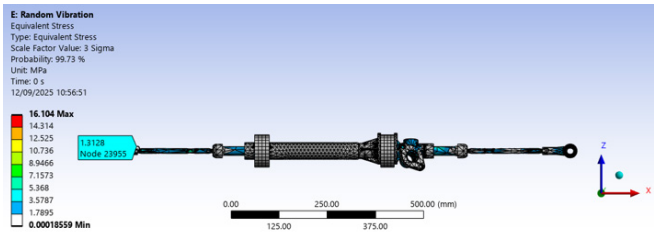


Figure 13. Equivalent von Mises stress distribution along the Z-axis

The analysis indicates a maximum stress of 1.131 [MPa], located at the threaded junction between the kingpin and the steering linkage, which represents a potentially vulnerable area from a structural standpoint. These findings are essential for identifying the critical regions of the assembly and have a direct influence on its fatigue life, durability, and overall performance under dynamic loading conditions.

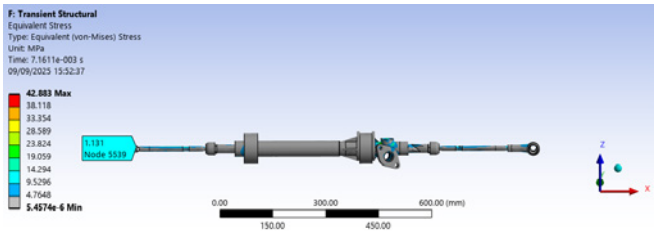


Figure 14. Equivalent von Mises stress distribution from the shock simulation

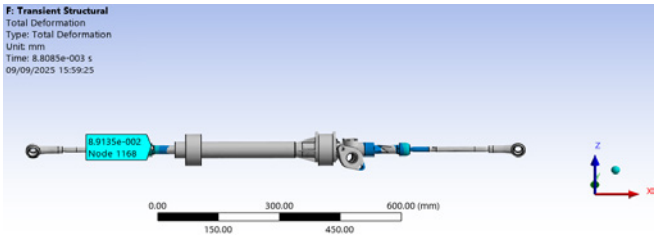


Figure 15. Total deformation distribution from the shock simulation

The deformation distribution across the entire steering assembly, as illustrated in Figure 15, provides a detailed view of the structural response under mechanical loading. This representation enables an in-depth evaluation of how the assembly reacts to dynamic forces, emphasizing regions where deformations are more pronounced and could influence the overall operational performance.

The simulation results indicate a maximum deformation of 8.913 × 10^{-2} [mm], located in the connection area where the steering linkage is mounted onto the steering gear rack. The accumulation of deformation in this critical region may compromise the functional stability of the assembly, potentially affecting the alignment and stiffness of interconnected components. Moreover, this structural behavior suggests an increased susceptibility to stiffness degradation over time, particularly under repeated or high-intensity loading conditions.

The previously performed simulations generated a series of graphs that emphasize the differences resulting from the geometrical enhancement of the steering rack with Kevlar bushings. These graphical results enable a comparative assessment between two configurations: the standard steering rack geometry and the Kevlar-reinforced configuration.

In total, five comparative plots are presented: three corresponding to the random vibration analysis, namely, the maximum directional acceleration, maximum directional deformation, and maximum equivalent stress and two derived from the shock (impact) analysis, representing the equivalent stress and the total deformation.

To further evaluate the impact of the proposed design modification, a comparative analysis was conducted between the standard steering rack geometry and the Kevlar-reinforced configuration. The following figures present the most relevant results obtained from the Random Vibration simulations, emphasizing how the integration of Kevlar bushings influences the dynamic behavior, vibrational response, and structural stiffness of the assembly.

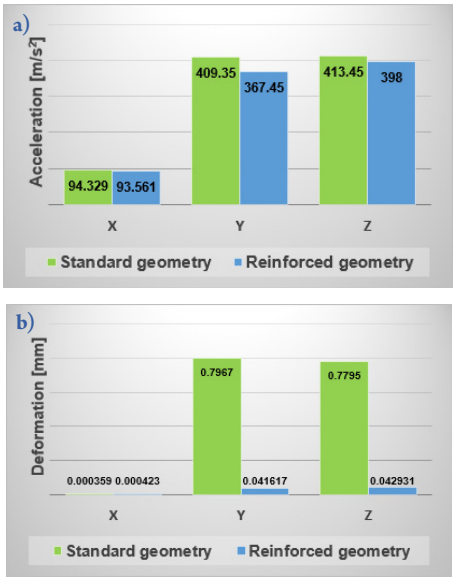


Figure 16. Maximum directional acceleration and deformation from Random Vibration simulations
a. Comparative directional acceleration from Random Vibration simulations
b. Comparative directional deformation from Random Vibration simulations

Figure 16.a illustrates the differences in directional acceleration observed in the Random Vibration simulations. The results indicate that the enhanced geometry, represented by the blue column, exhibits lower acceleration values across all analyzed directions compared to the standard configuration shown in green. This reduction in acceleration suggests that the Kevlar bushings effectively dampen dynamic excitations, contributing to improved stability and reduced vibrational loading on the steering assembly.

Figure 16.b presents the comparative directional deformation results obtained from the same Random Vibration simulations. In this case, the enhanced geometry demonstrates significantly lower deformation levels than the standard version, particularly in regions subjected to the highest

dynamic loads. This observation confirms the effectiveness of the Kevlar bushings in increasing the structural stiffness of the steering gear and limiting excessive deflections under vibrational excitation.

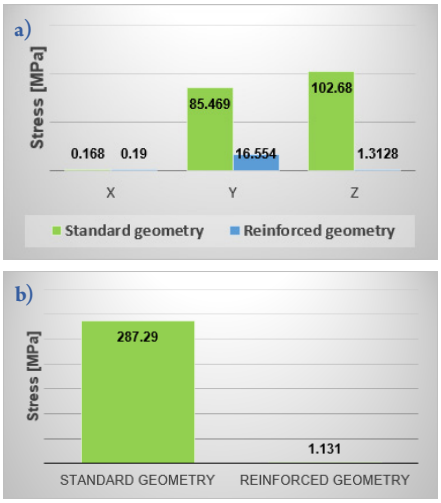


Figure 17. Maximum equivalent stress from Random Vibration and Shock simulations. a. Comparative maximum equivalent stress from Random Vibration simulations. b. Comparative maximum equivalent stress from Transient-Shock simulations

Figure 17.a presents the maximum equivalent stress values obtained from the Random Vibration simulations. The enhanced geometry, represented by the blue column, exhibits lower stress levels compared to the standard configuration, shown in green. This reduction in peak stress confirms the effectiveness of the Kevlar reinforcement in distributing mechanical loads more uniformly across the steering assembly, thereby reducing localized stress concentrations. These results demonstrate that
geometrical optimization can significantly improve the structural durability of the system under vibrational loading conditions.

Figure 17.b presents the maximum equivalent stress values obtained from the Transient-Shock simulations. The Kevlar-reinforced geometry, shown in blue, records lower peak stresses compared to the standard configuration, represented in green. This observation indicates that the Kevlar bushings effectively mitigate impact-induced stresses, improving the assembly's ability to withstand sudden dynamic loads. The results underline the structural advantages of the enhanced design, particularly in reducing potential failure risks and increasing overall reliability under transient loading conditions.

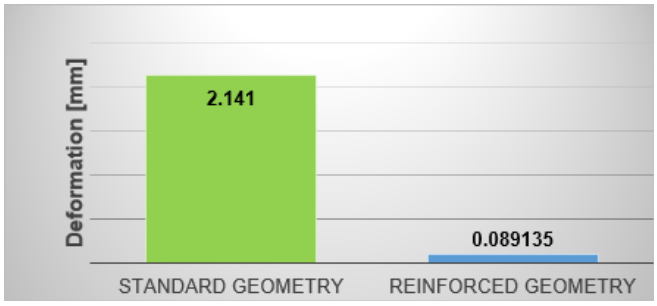


Figure 18. Comparative total deformation from Shock simulations

Figure 18 presents the total deformation results obtained from the Transient-Shock simulations. The enhanced geometry, represented by the blue column, exhibits lower deformation values compared to the standard configuration, shown in green. This reduction confirms that the Kevlar bushings improve the structural stiffness of the steering assembly, effectively limiting excessive displacements under sudden dynamic loads.

Due to the superior mechanical properties of Kevlar and the placement of the bushings in areas identified as critical, compared with the standard aluminum alloy solution, the simulation results at the critical nodes along the axis of maximum loading show reductions in acceleration values of up to 12.5% and reductions in deformations by more than an order of magnitude. This represents a particularly advantageous aspect in terms of driving safety, as it helps prevent, on the one hand, the occurrence of excessive clearances and, on the other hand, the risk of steering rack blockage due to seizure. Furthermore, this approach is considered to improve the service life of the steering rack assembly. At the same time, under shock loading, the equivalent stress can be reduced by up to 200 times at the nodes considered critical, and the deformations can be reduced by up to 24 times. The results highlight the beneficial effect of the Kevlar reinforcement in maintaining the alignment and stability of interconnected components, thereby contributing to the overall durability and reliability of the steering system under shock conditions.

4. CONCLUSION

The study demonstrated that the integration of Kevlar bushings into the mounting zones of an aluminum steering rack significantly improves its mechanical performance under dynamic loading conditions. The finite element simulations confirmed that the Kevlar-reinforced configuration effectively reduces peak stresses, deformations, and directional accelerations compared to the standard geometry.

These improvements result in enhanced vibration damping, increased structural stiffness, and superior energy dissipation during both random vibration and transient shock events. Consequently, the optimized steering rack exhibits greater durability, reliability, and operational safety, representing a viable solution for improving performance and extending the service life of modern automotive steering systems.

REFERENCES:

[1] *Popa, A. G.; Petrovan, Ș.; Rakosi, E.; Ulian, T. M. and Manolache, G., Evaluation of Steering System Performance Under Vibrational and Shock Loads Considering Influential Factors. Proceedings of the International Conference on Energy Systems 2025 (ICES-25);*
Yildiz Technical University, Istanbul, Türkiye; May 11–14, 2025.

[2] Li, W., *Application and Lightweight Research of New Aluminum Alloy Materials in Automotive Components. Academic Journal of Materials & Chemistry.* Francis Academic Press, 2025.

[3] Özbek, O., *Axial and lateral buckling analysis of Kevlar/epoxy fiber-reinforced composite laminates incorporating silica nanoparticles. Polymer Composites Journal.* Wiley, 2021.

Books:

[4] Lalanne, Christian, *Mechanical Vibration and Shock Analysis, Volume 1: Sinusoidal Vibration (3rd Edition).* Chichester, UK: Wiley, 2018.

[5] Zhang, Zhen; Richardson, Mark; Wisnom, Michael, *Structural Impact and Crashworthiness of Composite Materials.* Cambridge, UK: Woodhead Publishing (Elsevier), 2021.

[6] Pusey, Henry; Evans, David, *Shock and Vibration Standards.* In: *Harris' Shock and Vibration Handbook.* New York: McGraw-Hill, 2002.

[7] ANSYS, *https://www.ansys.com* Accessed on September 11, 2025.

[8] DELSERRO ENGINEERING SOLUTION *https://www.desolutions.com/testing-services/test-standards/iec-60068-2* Accessed on September 09, 2025.

[9] ISO, *Road vehicles - Environmental conditions and testing for electrical and electronic equipment -*
Part 3: Mechanical loads (ISO 16750-3). Geneva: International Organization for Standardization, 2012.

[10] SAE International, *Composite Materials Handbook, Volume 1: Polymer-Matrix Composites - Guidelines for Characterization of Structural Materials.* Warrendale, PA: SAE International, 2012.

MODAL ANALYSIS AND OPTIMIZATION OF TRUCK CABIN STRUCTURE

ANALIZA MODALĂ ŞI OPTIMIZAREA STRUCTURII CABINEI DE AUTOCAMION

ABSTRACT: *In this study, a modal analysis of truck cabin structure is performed to determine its main modes of vibration and critical frequencies. Modal analysis is used to characterize the dynamic behavior of the cabin structure by identifying its natural frequencies and mode shapes. Resonance occurs when the cabin structure is exposed to dynamic excitation whose frequency coincides with one of its natural frequencies.[5] Vibration modes are evaluated through natural frequencies or resonant frequencies as well as modal forms, which refer to the way the cabin truck structure deforms during vibration at a certain frequency. When the resonance occurs, vibrations could appear both over the entire structure and on a specific area or component of the cabin structure (i.e cross beam, walls, floor).[1] In this study, the truck cabin structure is modeled and analyzed in ANSYS using the finite element method to determine its modal characteristics. Using the sensitivity analysis of the first modal frequency as a reference, the cabin structure is optimized. The paper examines the behavior of a two truck cabin structures, a basic cabin without ribs on the wall panels and an optimized one (optimized by adding ribs to the wall panels) modeled to investigate their dynamic characteristics. The optimization of the truck cabin structure resulted in increase in the first-order vibration frequency, which rose from 17.62 Hz to 22.52Hz also the deformations significantly decreased as a result of this optimization.*

REZUMAT: *În acest studiu se realizează o analiză modală a structurii cabinei unui autocamion pentru a determina principalele sale moduri de vibrație și frecvențele proprii. Analiza modală este utilizată pentru a caracteriza comportamentul dinamic al structurii cabinei prin identificarea frecvențelor proprii și a formelor modale. Rezonanța apare atunci când structura cabinei este supusă unei excitații dinamice a cărei frecvență coincide cu una dintre frecvențele sale proprii. Modurile de vibrație sunt evaluate prin frecvențele naturale sau frecvențele de rezonanță, precum și prin formele modale, care descriu modul în care structura cabinei camionului se deformează în timpul vibrației la o anumită frecvență. [5] Când apare rezonanța, vibrațiile pot apărea atât asupra întregii structuri, cât și pe o anumită zonă sau un component specific al cabinei (de exemplu traversa, pereții sau podeaua)[1]. Structura cabinei camionului este modelată și analizată în ANSYS folosind metoda elementelor finite pentru a determina caracteristicile sale modale. Folosind analiza de sensibilitate a primei frecvențe modale ca referință, structura cabinei este optimizată. Lucrarea examinează comportamentul a două structuri de cabină de camion: una de bază, fără nervuri pe panourile laterale, și una optimizată (optimizată prin adăugarea de nervuri pe panourile laterale), modelate pentru a investiga caracteristicile lor dinamice. Optimizarea structurii cabinei camionului a dus la o creștere a primei frecvențe proprii de vibrație, care a crescut de la 17,62 Hz la 22,52 Hz, iar deformațiile s-au redus semnificativ ca urmare a acestei optimizări.*

Keywords: *truck cabin, vibration, optimization, modal analysis.*



Asist. univ. drd. ing.
Alexandra MOLEA



Conf. dr. ing.
Cornelia STAN



S.l. dr. ing.
Ana Maria DUMITRACHE

Universitatea Națională de Știință și Tehnologie Politehnica București, Departamentul de Autovehicule Rutiere, Splaiul Independenței 313, BUCUREȘTI, România

1. INTRODUCTION

When analyzing a vehicle body in white structure, it is essential to examine its NVH (Noise, Vibration and Harshness) characteristics, which is an important aspect in the design and development of vehicles. Ensuring the every component of the truck cabin meets its design specifications is crucial for preventing unexpected failures [1]. The overall stiffness of the cabin structure is an important design attribute in truck design.

Modal analysis is a methodology used to examine the dynamic behavior of structures in response under vibration excitation. The vibration modes help to evaluate the way the truck cabin structure deforms during vibration at a certain frequency [1]. This provides all the valuable information needed to strengthen the truck cabin structure in the design stage. Truck cabin vibration and noise can cause fatigue driving. The construction of a truck cabin is divided into several parts like frame(the main longitudinal and transverse frame members that provide the structural foundation for the CBIW), rear panel (the flat surface at the rear of the cab, which can be used for cargo or attachment points), side panels (the vertical panels that run along the sides of the cab), roof panel (the top surface of the cab that provides structural support and weather protection), windshield and side windows, door skins (the outer panels of the doors that provide additional strength and protection), B-pillar and C-pillar (the vertical pillars that connect the roof to the side panels) [2].

The purpose of this work is to analyze the behavior of a simplified truck cabin structure and an optimized truck cabin structure by adding ribs to the roof panel and rear panel. The optimization of the panels' ribs can be adopted to improve stiffness, strength, NVH (Noise, Vibration and Harshness) and crashworthiness.

2. METHODOLOGY

2.1 CAD Model

In this study, the geometric model of a heavy-truck day cabin is developed using ANSYS software. The main components of the truck cabin from a structural perspective are as follows: front wall, side walls, floor and roof. The truck cabin structure is constructed using sheet metal components, which are primarily welded together. The design of the cabin was accomplished directly in ANSYS, utilizing welded surfaces to create the overall geometry. Initially, the surfaces were created with thickness 0mm. Subsequently, each surface was assigned different thicknesses based on its layout and the structural requirements. Most parts have a thickness around 1 mm, and maximum thickness of less than 2.5 mm. This approach ensured that the cabin maintained optimal strength while minimizing weight, aligning well with the performance objectives of the truck. Various simulations and analyses were conducted to validate the integrity of the structure under various load conditions, contributing to a robust final design. For proposed work, two surface models were developed using ANSYS workbench to perform the modal analyses as shown in Figure 1.

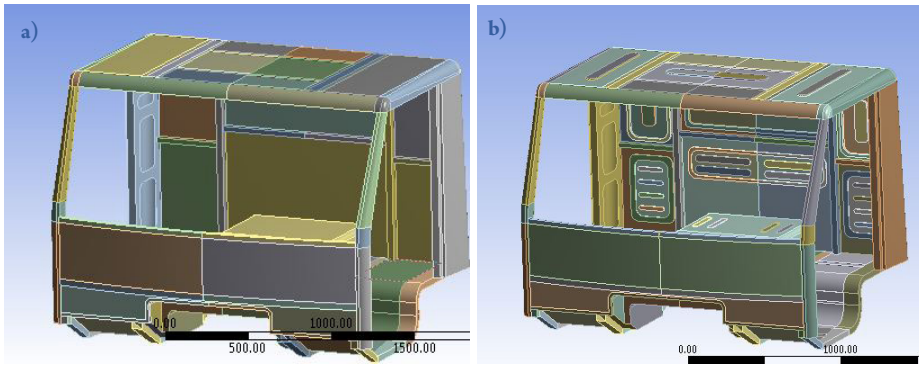


Figure 1 Surface Models of cabin structure a) model 1 the simplified cabin structure b) model 2 the optimized cabin structure

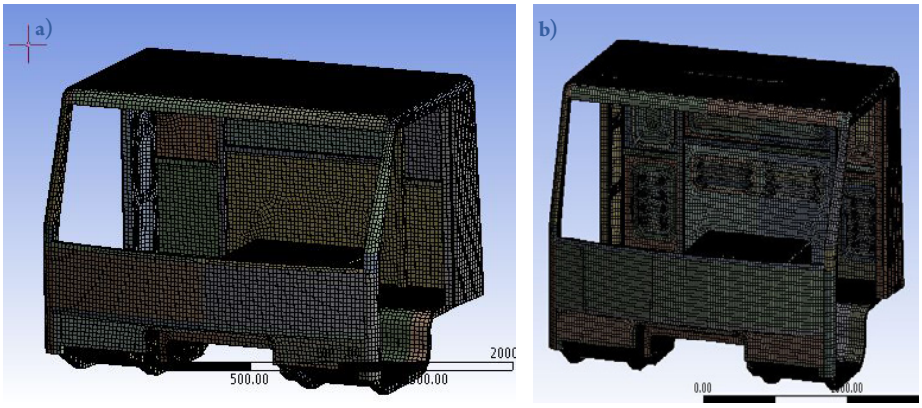


Figure. 2 Finite element model a) model 1 the simplified cabin structure b) model 2 the optimized cabin

2.2 Material modeling

In the analysis of the truck cabin, the same material is assigned to all profiles of the load-bearing structure. The material is selected from the ANSYS library with the following mechanical properties: Young's modulus E = 2 · 107 N / m2; Tensile Yield Strength: σ_c = 370 MPa, which are representative values for conventional structural steels used in vehicle cabin manufacturing.

The assumption of a uniform material is justified by industrial practice and the manufacturing technology of older-generation truck cabins, where cold stamping processes are used to reduce costs and increase production efficiency; consequently, a single steel grade is typically employed for the load-bearing structure, while local performance is enhanced through sheet thickness variations and reinforcement elements in critical areas.

This modeling approach is supported by manufacturer rescue documentation from the truck industry, such as Scania Rescue Cards, which show that stiffness variations in real truck cabins are achieved through geometric reinforcements and thickness variations rather than different base materials; therefore, assuming a homogeneous material allows the observed changes in natural frequencies to be directly attributed to the introduction of stiffening ribs[6]. During the optimization process, the overall mass of the cabin was monitored to ensure consistency with real structures. The total mass increased from 185.64 kg for the initial configuration to 187.23 kg for the optimized configuration, representing a negligible variation. This value remains within the range of the total mass measured on a real truck cabin, further validating the realism of the proposed finite element model.

2.3 Finite element methods

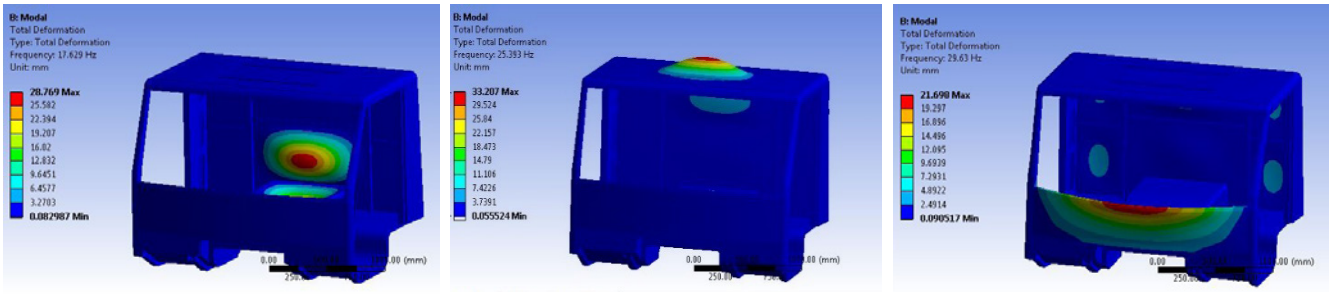
The finite element models of both the simplified and optimized truck cabins are generated using automatic meshing with quadrilateral and triangular elements to ensure accurate geometric representation and reliable structural analysis. Initially, all structural components were modeled as two-dimensional surfaces, and subsequently individual sheet-metal thicknesses were assigned according to structural and functional requirements. The thickness values were defined based on measurements performed on a real MAN truck cabin, ensuring a realistic representation of the actual structural configuration. Although different thickness values were used for specific components, the same material properties were maintained throughout the entire structure. The discretization of both cabin models was performed in ANSYS Workbench using an automatic meshing procedure suitable for thin-walled sheet-metal structures. Shell elements with mixed quadrilateral and triangular topology were employed to accurately capture both flat and curved regions of the geometry. For both models, the mesh sizing was controlled using the "Use Advanced Size Function: Curvature" option, ensuring a refined mesh in regions with higher curvature while maintaining a coarser mesh in relatively flat areas.

The main meshing parameters were set as follows: Minimum Element Size = 4.80 mm, and Maximum Face Size ≈ 24.88 mm, Curvature Normal Angle = 30°. Automatic mesh-based defeaturing was enabled to prevent the generation of excessively small elements caused by minor geometric details. Inflation layers were not applied, as the present study focuses on global modal characteristics rather than local stress evaluation. As a result of the discretization, the FE mesh of model 1 (simplified cabin structure) consisted of 31,534 nodes and 32,662 elements (Fig. 2a), while model 2 (optimized cabin structure with stiffening ribs) consisted of 52,505 nodes and 54,251 elements (Fig. 2b). The increase in the number of elements in the optimized model is associated with the added geometric complexity introduced by the stiffening ribs.

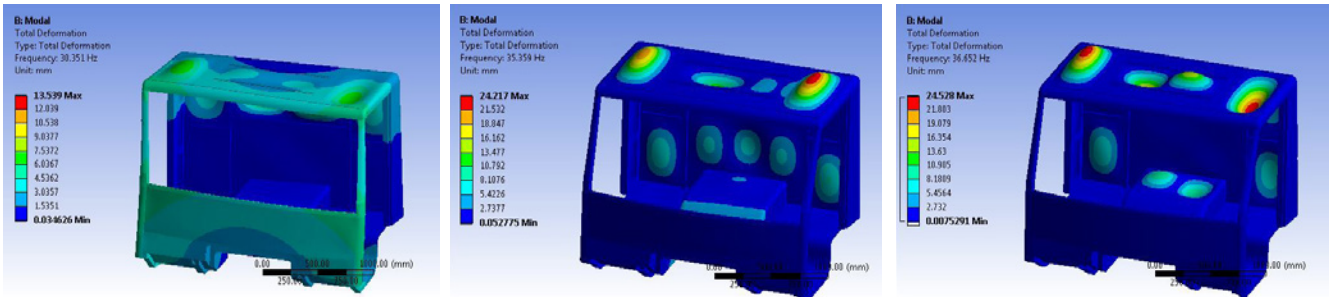
3. MODAL ANALYSIS REQUEST AND METHOD

Modal vibration modes are appreciated by natural frequency or resonant frequency, and by modal shape, which describes the way the body structure deforms during vibration at a certain frequency. When the resonance occurs, vibrations can manifest both throughout the entire cabin structure and on a specific zone or component of the cabin structure (for example beams, walls, floor, etc.) [3]. The most important natural vibration modes are those that have a resonant frequency throughout the entire structure. In this case, there are two resonant frequencies throughout the entire structure: the resonance frequency for bending and the resonance frequency for torsion [1].

The body is subjected to the free-free boundary conditions in ANSYS Workbench in the modal analysis module. This condition means that the cabin structure is free in space without any restriction or connections to



mode 1 mode 4 mode 7



mode 8 frequency of the overall torsional mode 10 mode 13

Figure 3 Modal shapes of the initial cabin structure

ground. Regarding the results obtained for the simplified cabin structure's response, Figure 3 and Table 1 the values of the resonant frequencies for the first 14 calculated natural modes.

Table 1
The results of first fourteen calculation mode

Order	Frequency [Hz]	Order	Frequency [Hz]
1	17,62	8	30,34
2	22,67	9	31,46
3	23,42	10	35,36
4	25,39	11	35,38
5	25,47	12	36,5
6	25,88	13	36,66
7	29,63	14	36,95

The first fourteen cabin modes were obtained from finite element modal analysis. The results obtained are consistent with the findings from previously manufactured cabins, thereby validating the accuracy of the 3D model and the simulation parameters employed in the analysis [4]. Natural vibration frequencies are presented in Table 1. The most important own vibration modes are those that exhibit a resonant frequency throughout the entire structure [3].

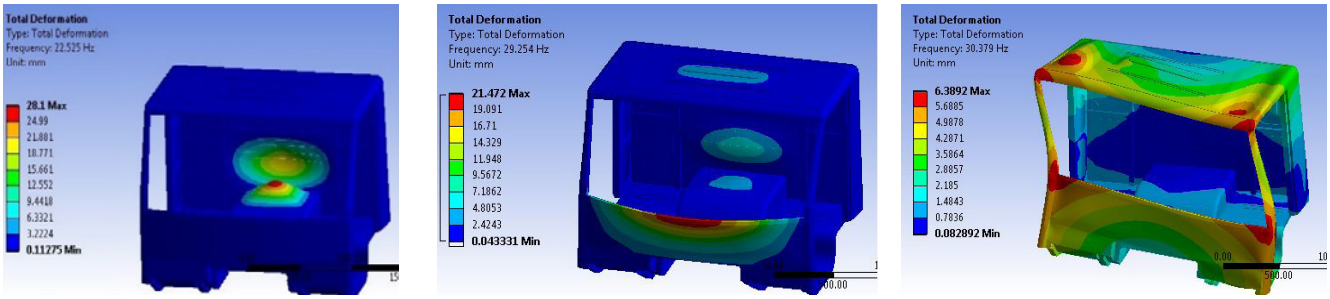
In this case, two resonant frequencies are found on the entire structure: the resonant frequency under bending and the resonant frequency under torsion. Following analysis and study of the cabin's structure, it was determined that the value of the resonant frequency of the overall torsional of the simplified cabin structure is 30,35 Hz at mode 7. Starting from the simplified structure, the structure was optimized by adding some ribs to the back walls, roof and floor. The topology optimization of the cabin structure can be seen in the Fig.1b. A free modal analysis is performed on the optimized cabin design, and its results are compared with those of the simplified cabin structure, as presented in Table 2.

Table 2
Modal frequency analysis of the initial and optimized cabin models

Order	Initial cabin	Optimized cabin	Order	Initial cabin	Optimized cabin
1	17,62	22,52	8	30,34	40,52
2	22,67	23,5	9	31,46	41,27
3	23,42	27,39	10	35,36	41,99
4	25,39	29,25	11	35,38	42,61
5	25,47	30,38	12	36,5	44,17
6	25,88	30,57	13	36,66	45,76
7	29,63	38,86	14	36,95	46,03

The first order vibration frequency rose from 17,62Hz to 22,52 Hz after modification, meeting the design requirement for a truck cabin structure. Table 2 shows that the first fourteen natural vibration frequencies of the optimized cabin structure are all higher compared to those of the simplified cabin structure, indicating an improvement in the modal stiffness of the optimized cabin. This can be seen in mode 5 (Fig. 5), where the frequency of the overall torsional appears at the value of 30Hz, but the total deformation decreased from 13.54mm to 6.39mm. After optimization the stiffness increased. The stiffness of a structure is a measure of its ability to resist deformation or deflection when subjected to an external force. A stiffer structure will exhibit a higher natural frequency than a less stiff one. This is because stiffness is directly related to the structure's resistance to motion.

As shown in Table 3, the optimization of the truck cabin structure leads to a significant increase in the first-order natural frequency, from 17.62 Hz to 22.52 Hz, corresponding to an improvement of approximately 27.8%. At the same time, the total mass of the cabin increases only slightly, by about 0.86%, remaining within the range of the mass measured for a real truck cabin.



mode 1 mode 4 mode 5 frequency of the overall torsional

mode 7 mode 12 mode 13

Figure 4 Modal shapes of the optimized cabin structure

Table 3
Comparison of results before and after optimization

Comparison parameter	Initial cabin	Optimized cabin	Variation
Total mass[kg]	185,64	187,23	+0.86%
First-order natural frequency [Hz]	17,62	22,52	+27.8%
Total deformation in torsional mode [mm]	13,54	6,39	−52.8%

These results indicate that the proposed geometric optimization, based on the introduction of stiffening ribs, effectively enhances the dynamic behavior of the cabin without a significant mass penalty. Consequently, the first natural frequency is shifted away from critical excitation ranges, reducing the risk of resonance phenomena.

4. CONCLUSION

In conclusion, the optimized cabin structure has a significant impact on the natural frequencies of the truck cabin. The comparison shows that the optimized cabin structure exhibits higher natural frequencies than the initial cabin structure for all orders (modes) considered. The optimization of the truck cabin structure resulted in a significant increase in the first-order vibration frequency, which rose from 17.62 Hz to 22.52 Hz, thereby fulfilling the design requirements. The optimized cabin exhibits consistently higher natural frequencies across all orders (1-14), indicating that the optimization process has improved the structural stiffness and damping properties of the cabin.

Consequently, the observed differences in natural frequencies are mainly attributed to the increase in structural stiffness induced by the introduction of stiffening ribs on the cabin panels, rather than to changes in material properties or total mass. This approach was adopted to highlight the importance and influence of the added ribs on the dynamic behavior of the studied models, while keeping the basic cabin structure unchanged.

ACKNOWLEDGEMENT

This work was supported by a grant from the National Program for Research of the National Association of Technical Universities - GNAC ARUT 2023.

REFERENCES:

[1] Iozsa D, *Studies on the real-time analysis of the behavior of bodies on impact, in order to improve the passive security offered to passengers*, Project ID-140, IDEI Program, Bucharest, 2009;

[2] Johansson I and Gustavsson M *2000 FE-based vehicle analysis of heavy trucks, Part I: Methods and Models*, proc of 2nd MSC. World-wide Automotive Conference, MSC (Sweden);

[3] Wang, X., Wang, D., Sun, W., Liu, P. (2013). *Lightweight Design and Evaluation for Cab-in-White of Heavy-Duty Truck*. In: Proceedings of the FISITA 2012 World Automotive Congress. Lecture Notes in Electrical Engineering, vol 196. Springer, Berlin, Heidelberg;

[4] Xiaomin, Qi, Ding Fang, and Xu Dezhang. *„Modal sensitivity analysis and structural optimization of the cab of light truck.“* 1st International Conference on Mechanical Engineering and Material Science (MEMS 2012). Atlantis Press, 2012;

[5] Iozsa D et al, *Study of the Dynamic Behaviour of the Car Body using Modal Analysis*, ESFA 2003 Conference, Bucharest, 2003

[6] Scania CV AB, *Scania Rescue Card – Next Generation Trucks*, Public Safety Documentation, Sweden

FUEL ECONOMY AND CO_2 EMISSION BENEFITS OF 48 V MILD HYBRID ARCHITECTURES (P0–P2)

ANALIZA BENEFICIILOR PRIVIND ECONOMIA DE COMBUSTIBIL ŞI EMISIILE POLUANTE PENTRU ARHITECTURILE *MILD HYBRID MHEV* DE 48 V (P0–P2)

ABSTRACT: *Over the past decade, the automotive industry has increasingly developed hybrid propulsion technologies to meet growing global demand for sustainable mobility. Mild hybrid electric vehicles (MHEVs) provide a cost-effective and practical compromise between conventional ICE vehicles and fully electric vehicles. This study reviews the classification of hybrid vehicles (MHEV, HEV, PHEV, and EREV) based on battery capacity, motor power, electric range, and functionality, emphasizing technical distinctions. Special focus is given to 48V MHEV systems and the influence of electric motor placement (P0–P2 architectures) on hybrid functionalities and efficiency. Through simulation of a C-segment MHEV under a WLTP driving cycle, differences in energy consumption, battery State of Charge (SOC) evolution, and CO_2 emissions are quantified. The findings highlight the strategic role of MHEVs in achieving a sustainable, economically, and technically viable automotive future.*

REZUMAT: *De-a lungul ultimului deceniu, industria auto a dezvoltat tehnologii hibride pentru a răspunde cererii tot mai mari de mobilitate sustenabilă. Vehiculele hibride electrice ușoare (MHEV) reprezintă o soluție practică între vehiculele convenționale cu motor cu ardere internă (ICE) și cele complet electrice. Studiul analizează clasificarea vehiculelor hibride (MHEV, HEV, PHEV și EREV) în funcție de capacitatea bateriei, puterea motorului electric, autonomia electrică și funcționalitate, evidențiind distincțiile tehnice și comparând avantajele și limitările MHEV-urilor. Se acordă atenție specială arhitecturilor 48V MHEV și poziționării motorului electric în lanțul cinematic (P0–P2) asupra eficienței și funcționalității hibride. Prin simulare pe un MHEV din segmentul C, în cadrul ciclului WLTP, lucrarea cuantifică diferențele de consum de energie, evoluția stării de încărcare a bateriei (SOC) și emisiile de CO_2. Concluziile subliniază rolul strategic al MHEV-urilor în susținerea unui viitor auto sustenabil, economic și tehnic viabil*

Keywords: *hybrid vehicle, 48V mild hybrid, electric motor, fuel economy, CO_2 emissions*



Drd. ing.
Elena-Daniela LUPU
elena.lupu@usm.ro



Prof. dr. ing.
Ștefan-Lucian TABACU

Universitatea Națională de Știință și Tehnologie Politehnica București, Departamentul Autovehicule și Transporturi, Str. Târgu din Vale, Nr.1, 110040 PITEȘTI, România

1. INTRODUCTION

The automotive industry has been continuously progressing hybrid propulsion technologies to address the growing global demand for sustainable mobility and strict greenhouse gas emission regulations for the past decade [1][2]. Today, hybrid vehicles are transitional solution between conventional internal combustion engine (ICE) vehicles and fully electric vehicles, combining extended driving range with reduced environmental impact and mitigating the range anxiety associated with pure electric vehicles [1][3].

Hybrid vehicles, also known as partially electric vehicles, integrate an ICE with an electric motor (EM) in the drivetrain. They are classified according to their level of electrification, which reflects the electric motor's contribution to propulsion. The main categories are Mild Hybrid Electric Vehicle (MHEV), Hybrid Electric Vehicle (HEV), Plug-in Hybrid Electric Vehicle (PHEV), and Extended Range Electric Vehicle (EREV, a subset of PHEV with extended electric range) [2][3].

Mild Hybrid Electric Vehicles (MHEVs) offer a cost-effective alternative to more complex hybrid technologies [1][2][4]. They incorporate a small electric motor, typically powered by a 48 V lithium-ion battery, to assist the ICE during high-load conditions such as engine start-up and acceleration [4][5][6]. MHEVs feature regenerative braking but cannot propel the vehicle solely with electric power for extended distances [2][3]. This configuration improves fuel efficiency and reduces emissions while avoiding complexity and higher costs of full or plug-in hybrids [1][5][7].

This study systematically analyzes hybrid vehicle powertrain architectures, focusing on technical parameters that influence the degree of hybridization and drivetrain efficiency. Special attention is given to the physical integration of the electric motor within the powertrain and its impact on regenerative braking, drivability, and compatibility with advanced features such as all-wheel drive and torque vectoring [4][7][8]. Comparative analyses with other hybrid technologies contextualize the advantages and limitations of MHEVs.

Through simulation and comparative testing of a C-segment MHEV under a WLTP driving cycle, differences in energy consumption, battery State of Charge (SOC) evolution, and CO_2 emissions are quantified across P0, P1, and P2 architectures. The findings highlight the strategic role of MHEVs in supporting a sustainable, economically feasible, and technically robust pathway for the automotive industry's transition toward electrification [1][9][10][11].

2. OVERVIEW OF HYBRID VEHICLE POWERTRAIN ARCHITECTURES

Due to the combination of the internal combustion engine and the electric motor, hybrid vehicles exhibit a more complex architecture than conventional vehicles, and their classification into MHEV, HEV, PHEV, and EREV categories depends on several key factors that reflect the degree of electrification of the propulsion system [2][3].

The fundamental technical factors used to evaluate the electrification level and the complexity of the hybrid powertrain, as well as the vehicle's energy and functional performance, are:

- ✓ *battery capacity* indicates the amount of electrical energy the vehicle can store to power the electric motor. MHEVs use small batteries

Table 1.
Battery specifications for different hybrid configurations

Hybrid type	Battery capacity [kWh]	Battery chemistry	Voltage range [V]	Common chemistries	Example vehicles
MHEV	0.2 – 1.5	Li-ion NiMH (older)	12 – 48	LTO -rare, NMC-common	Audi A6 MHEV, Ford Puma Hybrid
HEV	1.0 – 2.0	NiMH, Li-ion	100 – 300	NMC-main NiMH -legacy, LFP -emerging	Toyota Prius, Honda Accord Hybrid
PHEV	8 – 20	Li-ion	300– 400	NMC -main LFP-increasing NCA -premium	Volvo XC60 Recharge, BYD Qin Plus DM-i
EREV	10 – 25	Li-ion	300– 400	NMC, NCA, LFP	BMW i3 REx, Chevrolet Volt

Table 2.
Main characteristics of electric motors across different hybrid vehicle categories

Hybrid type	EM type	EM power [kW]	Degree of hybridization [%]	EM torque [Nm]	max speed [rpm]	Vmax in EV mode [km/h]	Key functions
MHEV	PMSM, BLDC	5 – 20	5 -15	20 – 60	3,000 – 10,000	< 50 (assist)	start-stop, regenerative braking, torque assist, engine smoothing
HEV	PMSM	30 – 70	20 – 40	100 – 250	10,000 – 15,000	~60 (short EV)	EV mode at low speeds, regenerative braking, hybrid propulsion
PHEV	PMSM, occasionally AC Induction	50 –100+	40 – 70	200 – 400	10,000 – 18,000	>100 (EV mode)	extended EV mode, hybrid drive, plug-in charging, regen braking
EREV	PMSM	50 – 120	100%	250 – 500+	12,000 – 18,000	>120 (EV mode)	full EV mode, ICE acts as generator, extended range after battery depletion

Table 3.
Battery specifications for different hybrid configurations

Hybrid type	Electric range [km]	Charging time (AC, 3.7–7 kW)	Example vehicles
MHEV	0	N/A (no plug-in)	Audi A4 12V MHEV, Ford Puma MHEV, Mercedes-Benz C-Class MHEV, Volkswagen Golf 48V MHEV, BMW 3 Series MHEV
HEV	~1–3	N/A (no plug-in)	Toyota Corolla Hybrid, Honda CR-V Hybrid, Lexus RX 500h, Ford Escape Hybrid, Hyundai Tucson Hybrid
PHEV	30–100	2–4 hours	Volvo XC60 Recharge, Ford Escape PHEV, BYD Qin Plus DM-i, Mitsubishi Outlander PHEV, BMW X5 xDrive45e
EREV	~100–120	3–6 hours	BMW i3 REx, Cadillac Lyriq (EREV variant), Chevrolet Volt (recent), Fisker Ocean (EREV planned), Karma Revero GT

(typically under 1 kWh), sufficient only for limited functions such as start–stop operation and acceleration assistance. HEVs and PHEVs are equipped with medium- to large-capacity batteries that enable pure electric driving over varying distances. EREVs also use large batteries similar to those in PHEVs, but their internal combustion engine operates exclusively as a generator [1][2][3]. Table 1, based on battery specifications, provides a structured overview of the defining attributes for the four-hybrid vehicle category

✓ *electric motor power:* The motor's power relative to the internal combustion engine (ICE) output indicates the degree of hybridization. MHEVs are equipped with low-power electric motors (approximately 10–20 kW) that help but cannot propel the vehicle independently. HEVs and PHEVs, on the other hand, feature higher-power electric motors (ranging from 30 kW to over 100 kW), enabling pure electric driving over short or extended distances [3] [4][7]. Table 2 summarizes the main characteristics of the four hybrid vehicle categories from this perspective.

✓ *pure electric range:* This reflects how far the vehicle can travel using only the electric motor, without engaging the combustion engine. MHEVs generally do not provide a sustained pure electric driving mode, HEVs

allow only short electric operation, while PHEVs and EREVs enable significantly longer electric range due to higher battery capacity and system design [2][3]. Table 3 summarizes the main characteristics of the four hybrid vehicle categories from this point of view.

✓ *available functionalities:* include functionalities specific to each category, such as external charging capability (available in PHEVs and EREVs), regenerative braking, start–stop systems, torque assist, and extended electric-only driving modes [1][2][3][5].

From a different perspective, hybrid vehicles can be classified as series, parallel, or series-parallel), depending on whether the internal combustion engine and electric motor provide power to the wheels separately, together, or through a combination of both.

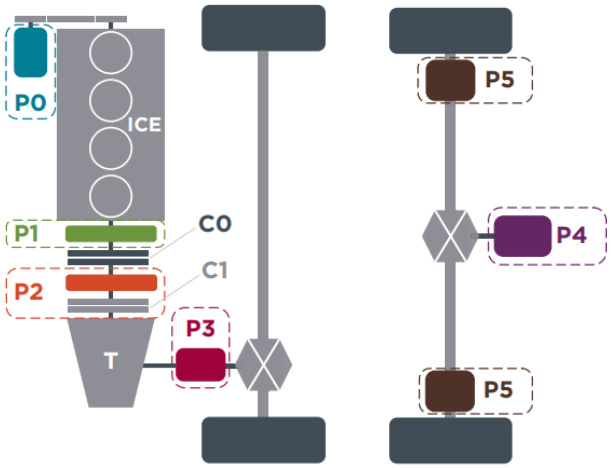


Figure 1. P0-P5 architectures of parallel hybrid vehicles [1][4][7].
ICE- internal combustion engine, C0, C1 – clutch, T – transmission, P0-Belt Starter Generator (BSG); P1- Crankshaft-mounted e-machine (ISG pre-clutch); P2 - E-machine between engine and gearbox (post-clutch); P3 -E-motor on driveshaft; P4 - E-machine on rear axle; P5 - Wheel hub motors

Research shows that hybrid configurations consistently reduce fuel consumption and CO_2 emissions compared to conventional ICE vehicles, with 48 V mild hybrid systems providing a strong cost-benefit ratio for near-term emission reduction[1][5][7].

Hybrid vehicles with a parallel drivetrain can be classified based on the physical position of the electric motor within the powertrain configuration. This P0–P5 classification indicates the location of the electric motor relative to the ICE, clutch, transmission, and drive axles and is widely used in the technical literature and industry practice. Each position directly affects the possible hybrid functionalities, such as the ability to drive in pure electric mode, regenerative braking capabilities, engine start/stop functionality, coasting with the ICE decoupled, electric assist during acceleration (boost) and compatibility with all-wheel drive (AWD) configurations, particularly when the EM is mounted on the axle not powered by the ICE [4][7][8]. Therefore, although the EM position does not directly determine the degree of electrification (MHEV, HEV, PHEV, EREV), it strongly influences which hybrid strategies and functions can be implemented in the powertrain system [7][9][10]. In summary, although the P0–P5 classification does not strictly define the vehicle's hybrid category, it strongly correlates with the electric motor's operational role and achievable performance functions across mild and full hybrid implementations.

3. ENERGY EFFICIENCY AND CO_2 EMISSIONS OF MILD HYBRID ELECTRIC VEHICLES

The comparative analysis was conducted using a MATLAB/Simulink simulation framework, in which the vehicle longitudinal dynamics and the hybrid powertrain components were modeled to reproduce the WLTP driving cycle. The study evaluates three 48 V mild-hybrid topologies (P0, P1, and P2) under identical vehicle and environmental conditions, while varying the electric machine placement and associated hybrid functionalities.

A C-segment passenger vehicle with a total mass of 1500 kg was considered. Longitudinal resistance forces were modeled using rolling resistance and aerodynamic drag. The road-load parameters were set to: rolling resistance coefficient $f_r = 0.014$, aerodynamic drag coefficient $C_x = 0.29$, frontal area $A = 2.2\ m^2$, air density $\rho = 1.2\ kg/m^3$, and ambient temperature 27°C. The vehicle speed trajectory was imposed by the WLTP cycle, and the model computed the corresponding traction power demand as a function of speed and acceleration, including road-load losses.

The vehicle is equipped with a 1.5 L turbocharged spark-ignition (SI) gasoline engine, rated at approximately 75 kW and 200 Nm peak torque. Engine operation was represented in a map-based manner (quasi-static steady-state approach), with an assumed peak brake thermal efficiency of approximately 35% (used as a reference efficiency level for the operating region relevant to WLTP). Fuel consumption was computed from the engine operating point and the required mechanical power delivered to the drivetrain.

- A 48 V electric machine was integrated according to each architecture. Electric assist and regenerative braking were modeled as power-limited functions constrained by the architecture and control strategy. The hybrid subsystem parameters were:P0: crankshaft-mounted 48 V machine, 10 kW / 65 Nm, providing up to 15% torque assist and up to 20% regenerative contribution.
- P1: pre-clutch 48 V machine, 15 kW / 80 Nm, enabling increased assist and engine-off operation at low speeds (limited electric operation where supported) and up to 50% energy recovery.
- P2: post-clutch machine between clutch and transmission, 25 kW / 150 Nm, enabling low-speed electric drive capability (below 60 km/h), coasting (engine decoupling), and maximum regenerative braking potential (up to the imposed control and power limits, nominally considered up to 100% of the available braking energy within constraints).

Electrical energy consumption and recuperation were tracked over the WLTP cycle, allowing direct comparison of net battery energy use for each topology.

A rule-based supervisory energy management strategy was implemented to coordinate engine operation, electric assistance, and regenerative braking under WLTP conditions. The strategy prioritizes electric torque assistance during engine-on operation to reduce engine load peaks, while commanding regenerative braking during deceleration phases subject to architecture-specific limits. For the analyzed cases, an "ICE-only" mode is not observed because electric assist is activated whenever the ICE is operating, leading to predominant hybrid-assist operation across all architectures.

For each hybrid configuration, the simulation reports: fuel consumption (L/100 km), electrical energy used and regenerated (kWh), CO_2 emissions (g/km), and time-resolved operating states including power flow distribution and SOC evolution.

Figure 2 shows that as hybrid architecture progresses from P0 to P2, the electric motor contribution to both propulsion assist and regenerative braking increases significantly, creating greater potential for engine-off operation and reduced ICE load, which improves overall energy efficiency and emissions performance.

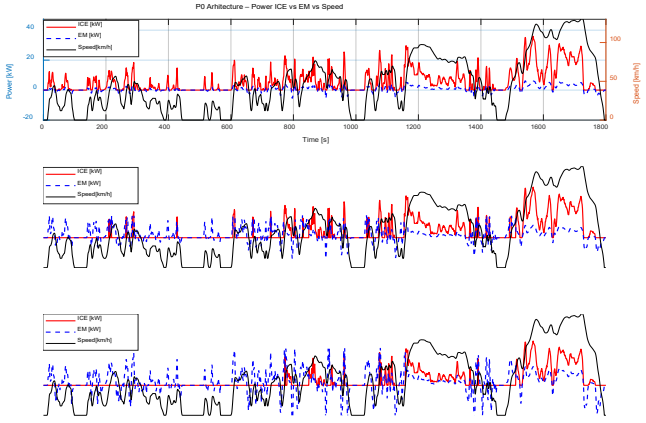


Figure 2. Comparative power profiles of ICE and EM for P0, P1 and P2 architectures

In the P0 architecture, the internal combustion engine provides most of the propulsion power throughout the WLTP cycle, while the electric motor delivers limited boost during acceleration and modest regenerative breaking, with virtually no electric-only operation.

In the P1 architecture, the electric motor plays a more important assist role, supporting propulsion and regenerative braking and enabling limited engine-off operation at low speeds, thereby reducing average ICE load compared to P0.

In the P2 architecture, the electric motor contribution is the most extensive, supporting frequent assist phases, stronger regenerative braking, and low-speed electric drive capability, with the ICE inactive during multiple WLTP intervals, resulting in the highest hybrid effectiveness among the three configurations.

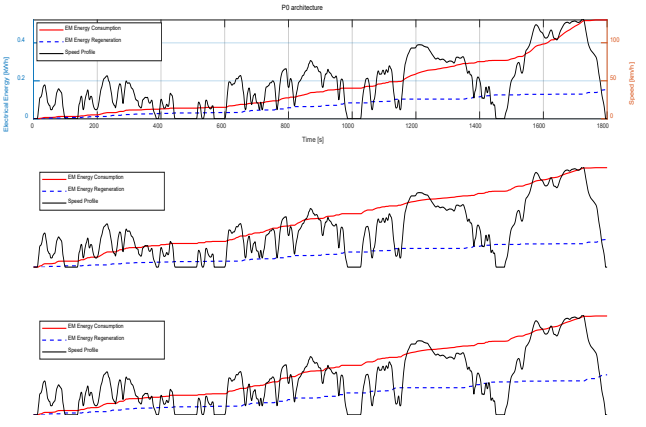


Figure 3. Electric motor energy consumption and regeneration profiles for P0, P1 and P2 architectures on WLTP cycle

As the hybrid system evolves from P0 to P2 (Figure 3), both electric energy consumption and regenerative energy recovery increase significantly. In all cases, consumed electrical energy exceeds regenerated energy, while the P2 architecture shows the highest value among the analyzed configurations due to its superior electric drive integration and regenerative capability. The graph analysis highlights clear differences among the three mild-hybrid architectures. The P0 configuration exhibits low and intermittent regenerative power peaks and a slow accumulation of recovered energy, indicating limited regenerative performance. The P1 architecture demonstrates moderate regenerative capability, with more frequent and higher recovery peaks, leading to increased recuperated energy. The P2 architecture shows the strongest regenerative behavior, characterized by pronounced peaks and sustained recovery intervals, resulting in the highest total recovered energy. Regenerative performance therefore improves progressively from P0 to P1 and reaches its maximum in P2.

The graphs in Figures 4a and 4b illustrate the WLTP-based evolution of fuel and electrical energy consumption normalized per 100 km, together with the instantaneous total power demand for the three hybrid architectures. The P0 configuration shows the highest power peaks and the largest average demand, indicating stronger reliance on the internal combustion engine. The P1 and P2 architecture exhibit progressively lower and smoother power profiles, with P2 achieving the greatest reduction in overall energy consumption due to its improved engine decoupling capability and more effective utilization of the electric drive. Overall, the transition from P0 to P2 demonstrates a clear improvement in hybrid efficiency and power management.

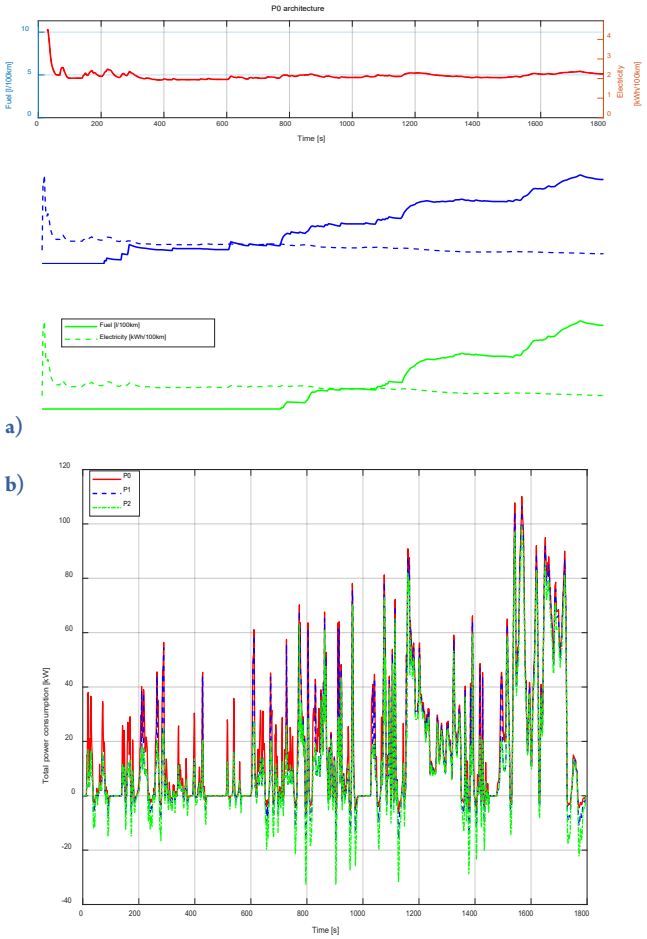


Figure 4. WLTP-based energy consumption and power response for P0, P1, and P2 MHEV architectures
a) Cumulative fuel and electrical energy consumption; b) instantaneous ICE–EM power profiles

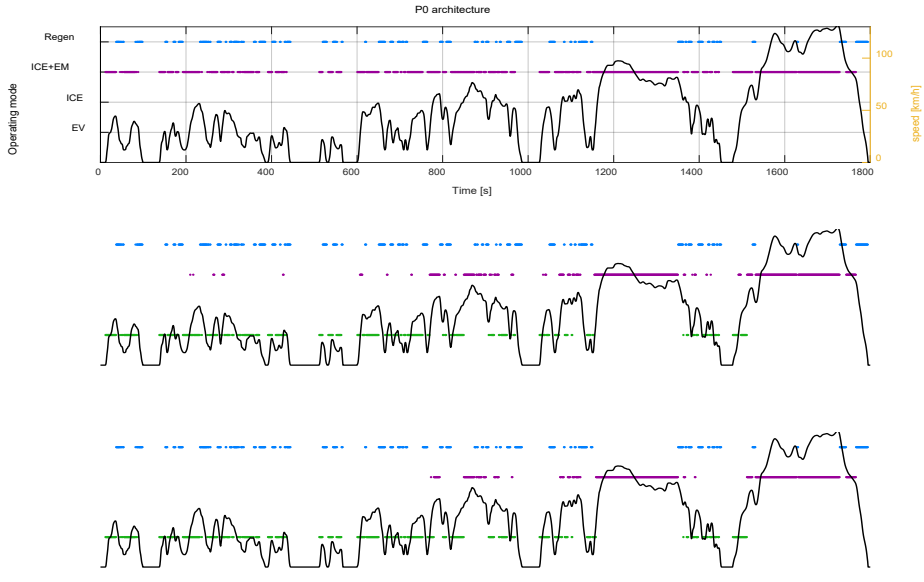


Figure 5. WLTP operating modes of P0–P2 hybrid powertrains

In the P0 architecture, the system operates primarily in ICE+EM assist mode, providing frequent electric boost but not enabling pure electric driving, with regenerative breaking occurring only during deceleration phases. The P1 configuration shows limited engine-off or low-speed electric operation (where supported), with more frequent transitions between ICE and hybrid assist modes, as well as increased regenerative events in urban driving segments. The P2 architecture achieves the most extensive electric drive utilization and regenerative braking capability, enabling repeated low-speed EV operation and effective ICE decoupling, particularly under stop-and-go conditions.

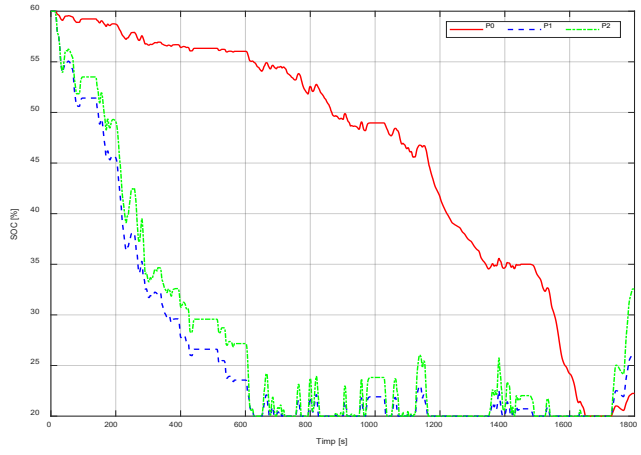


Figure 6. SOC evolution during WLTP Cycle – MHEV architectures

In the analysis shown in Figure 5, the "ICE-only" operating mode does not appear, since the implemented energy management strategy commands electric assist whenever the internal combustion engine is running. As a result, propulsion occurs predominantly in hybrid assist mode, improving overall efficiency and enabling regenerative capability across all three architectures

The C-segment MHEV vehicle considered in this analysis uses a 48 V, 17 Ah Li-ion battery representative of current-generation MHEV systems. Such systems typically operate within a state-of-charge window of approximately 20–80%, allowing both regenerative braking and electric assist while preserving cell durability. In production calibrations, the initial SOC is commonly set around 60%, since the mid-range region (about 40–70%) reduces electrochemical stress and cyclic aging. Initializing the SOC at 60% therefore reflects realistic energy management practice in modern MHEV architecture. The SOC evolution shown in Figure 6 highlights distinct behavior across the three architectures. In the P0 configuration, SOC decreases gradually over the WLTP cycle, indicating moderate electric assist usage without sustained electric drive operation, and remains above the lower SOC bound for most of the test duration. In the P1 architecture, SOC drops rapidly in the early phase of the cycle due to more frequent electric assistance and engine-off operation at low speeds, reaching the minimum SOC threshold relatively early and remaining close to this constraint thereafter.

The P2 architecture shows the fastest SOC depletion, consistent with its higher electric drive utilization and stronger regenerative interaction, causing the battery to reach the lower SOC limit shortly after the start and remain near that bound, with only minor recovery episodes.

Under WLTP conditions, all architectures approach the lower SOC limit (~20%) before the end of the cycle, indicating that the selected battery capacity is sufficient for a full WLTP run but provides limited additional electric operating margin. The modest SOC recovery observed suggests either limited regenerative energy opportunities within the WLTP profile or control and charging power constraints associated with the battery and converter sizing.

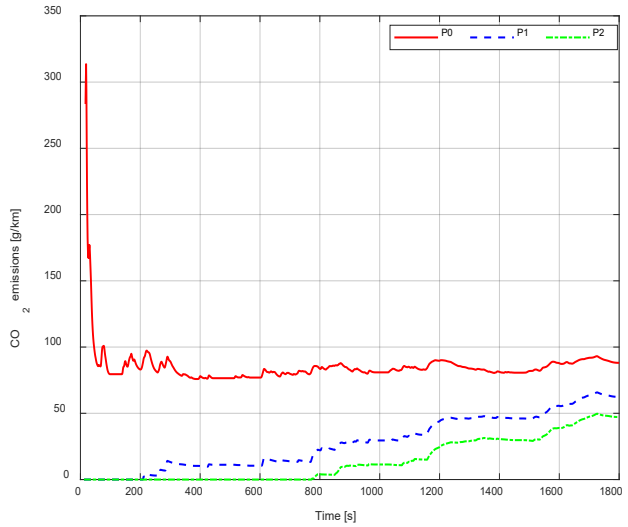


Figure 7. WLTP CO_2 emissions and normalized energy performance comparison for P0, P1, and P2 MHEV architectures

The CO_2 emission results for the three hybrid architectures (P0, P1, and P2) shown in Figure 7 were compared with recent European MHEV fleet averages for 2024. Although official fleet statistics are not architecture-resolved, it is widely recognized that average emissions decrease as more advanced hybrid layouts (P1 and especially P2) gain market share.

The WLTP emission profiles in Figure 7 (left) show a clear separation between the three configurations over the entire cycle. The P0 architecture maintains the highest CO_2 level throughout most of the test, with relatively limited dynamic reduction capability, whereas P1 and P2 exhibit substantially lower and more stable emission trajectories after the initial transient phase. The P2 curve remains consistently lowest, confirming the stronger electric contribution and more effective engine load reduction.

The normalized comparison in Figure 7 (right) further quantifies these differences: CO_2 emissions decrease from about 88.1 g/km for P0 to 62.4 g/km for P1 and 47.2 g/km for P2, corresponding to an overall reduction of roughly 46% between P0 and P2. This trend is consistent with the simultaneous reduction in fuel consumption and the increase in electrical energy utilization observed across the architecture.

The P2 configuration achieves emission levels well below the latest reported fleet average (approximately 102 g/km for MHEVs in 2024), confirming the effectiveness and competitiveness of the implemented energy management strategy. The P1 architecture also performs significantly below the fleet benchmark, while even the P0 configuration remains below the current market average despite its more limited hybrid functionality.

Overall, the results demonstrate that progressive hybrid architecture enhancement combined with optimized supervisory control yields substantial CO_2 emission benefits under WLTP conditions, with P2 approaching emission levels typically associated with higher electrification classes, despite the absence of external charging capability.

This emission trend is consistent with the normalized consumption results shown in Figure 7, where fuel consumption decreases from P0 to P2 while electrical energy utilization increases, confirming that CO_2 reduction is primarily driven by fuel displacement through electric assist and regenerative operation.

4. CONCLUSIONS

The comparative WLTP-based simulation of three MHEV architectures (P0, P1, and P2) highlights significant differences in energy consumption and CO_2 emissions, driven by both hybrid topology and supervisory energy management strategy. Among the analyzed configurations, the P2 architecture consistently achieved the lowest fuel consumption and CO_2 emissions, reaching values below current European MHEV fleet averages and approaching the performance range typically associated with full hybrid vehicles under standardized test conditions. The P0 and P1 results are consistent with earlier-generation MHEV systems and confirm the progressive improvement in efficiency and emission reduction with increasing electrification level and regenerative capability.

Although P2 remains a mild hybrid architecture, the combination of higher electric motor capability and optimized control enables emission performance that approaches that of some full hybrid systems in WLTP operation. This indicates that, under certain driving cycles and with effective control calibration, the performance gap between advanced MHEV and HEV configurations can be substantially reduced, even without large battery capacity or plug-in functionality.

The analyzed SOC trajectories, propulsion mode distributions, and instantaneous power flows confirm that frequent electric assist, strong regenerative utilization, and engine-off operation at low speeds are key contributors to minimizing fuel consumption and CO_2 emissions in mild hybrid powertrains.

Comparison with published fleet statistics for 2020–2024 supports the plausibility and representativeness of the simulation results and suggests that next-generation P2-oriented MHEV designs can approach the lower bound of current hybrid fleet emission levels.

Overall, the study demonstrates that, beyond hardware architecture, control strategy optimization plays a decisive role in achieving high efficiency and low emissions in modern MHEVs. Mild hybrid systems represent a cost-effective and low-complexity pathway for CO_2 reduction in transitional markets. While their absolute impact remains below that of full hybrids and battery electric vehicles, MHEVs contribute meaningfully to fleet-wide emission compliance and serve as an effective intermediate step toward deeper electrification.

REFERENCES:

[1] J. Dornoff, J. German, A. Deo, and A. Dimaratos, *Mild-hybrid vehicles: A near term technology trend for CO2 emissions reduction*, The International Council on Clean Transportation (ICCT), July 4, 2022.

[2] D. S. Cardoso, P. O. Fael, and A. Espírito-Santo, *A review of micro and mild hybrid systems*, Energy Reports, vol. 6, suppl. 1, pp. 385–390, 2020. doi:10.1016/j.egyr.2019.08.077

[3] Pundir and A. Saini, *Mild hybrid technology in automotive: A review*, International Journal of Engineering Research & Technology (IJERT), vol. 8, 2021.

[4] M. Melaika, S. Mamikoglu, and P. Dahlander, *48V Mild-Hybrid Architecture Types, Fuels and Power Levels Needed to Achieve 75 g CO_2/km*, SAE Technical Paper 2019-01-0366, 2019.

[5] H. Oh, J. Lee, S. Woo, and H. Park, *Effect of synergistic engine technologies for 48 V mild hybrid electric vehicles*, Energy Conversion and Management, vol. 244, 2021, Art. no. 114515.

[6] U.S. EPA, *Modeling and Controls Development of 48 V Mild Hybrid Electric Vehicles*, SAE Paper, 2018.

[7] Y. Liu, Y. G. Liao, and M.-C. Lai, *Fuel economy improvement and emission reduction of 48 V mild hybrid electric vehicles with P0, P1, and P2 architectures with lithium battery cell experimental data*, Advances in Mechanical Engineering, vol. 13, no. 10, 2021, Art. no. 16878140211036022. doi: 10.1177/16878140211036022.

[8] B. McKay (Continental AG), *Benefits of a 48 V P2 Mild Hybrid*, ACC Symposium, sept. 2016.

[9] J. J. Eckert, S. F. da Silva, M. A. de Menezes Lourenço, F. C. Corrêa, L. C. A. Silva, and F. G. Dedini, *Energy management and gear shifting control for a hybridized vehicle to minimize gas emissions, energy consumption and battery aging*, Energy Conversion and Management, vol. 240, Art. no. 114222, 2021.

[10] M. Shang, Z. Zhang, C. Yin, and K. Li, *The development of the fuel saving control strategy for 48 V P0 system: Design and experimental investigation*, Advances in Mechanical Engineering, vol. 16, no. 1, 2024.

[11] P. K. Chinthoju and R. S. Vashishta, *Well-to-Wheel Efficiency and Energy Consumption Analysis for Mild Hybrid Electric Vehicles*, J. Eng. Res. Rep., vol. 27, no. 2, pp. 216–227, Feb. 2025.

KART LOW COST 2026

– Wednesday –

// 14:00 pm

Oral presentations during the afternoon (≈3 hours)
10min presentation + 10min Q&A
Mid-competition results
Kart design review

Amphitheatre 1 - ISAT

49 rue Mademoiselle Bourgeois
58000 NEVERS

// 17:30 pm

Evening meal all together to meet everyone
// 19:00 pm

– Thursday –

// 8:30 am

Arrival at the track at 8:30

Circuit de karting de Magny-Cours

// 9:00 am

KLC Challenge starts at Magny-Cours track

61 route du circuit
58490 Saint-Parize-le-Châtel

// 14:00 pm

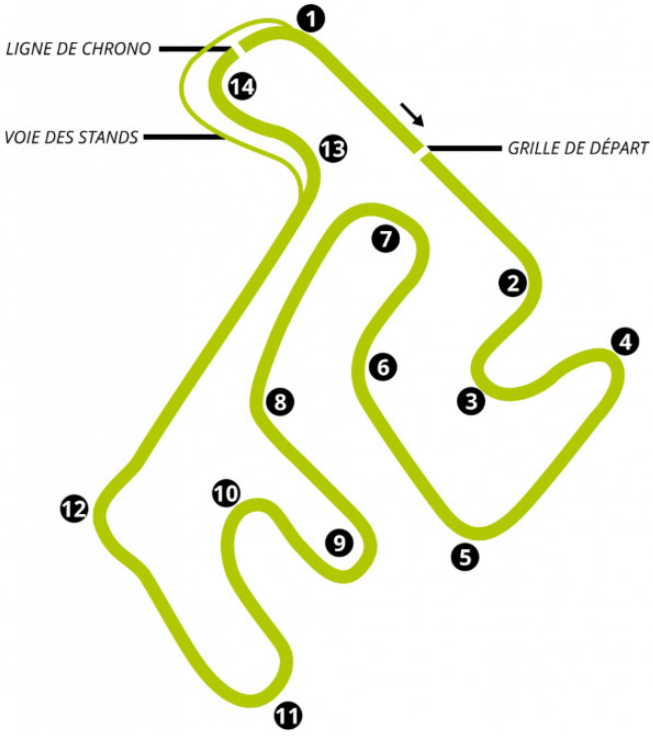
Results and awards ceremony
// 15:00 pm

Cea de-a paisprezecea ediție a concursului internațional studențesc Challenge Kart Low Cost s-a desfășurat la Institutul Superior de Automobile și Transporturi (ISAT) din Nevers, Franța în zilele de 6 și 7 mai 2026, ca de obicei, sub patronajul Societății Inginerilor de Automobile din România (SIAR).

În prima zi, studenții participanți au prezentat proiectele tehnice în cadrul ISAT, iar în a doua zi aceștia au concurat pe circuitul de karting situat la Magny-Cours, un circuit cu o lungime de 1100 m, între 8 – 10 m lățime, 14 viraje, dotat cu sistem profesionist de cronometrare.

Challenge Kart Low Cost s-a născut din nevoia de a crea o competiție centrată pe student care îmbină într-un mod optim teoria și practica, și care este gândită să reproducă în timpul studiilor universitare viața reală a unui inginer dintr-un centru de dezvoltare autovehicule. Așadar, în perioada octombrie – aprilie a anului academic, respectând constrângerile impuse printr-un caiet de sarcini[1], studenții dezvoltă un kart cu care concurează pe un circuit adecvat în luna mai.

Într-un asemenea proiect, asumat voluntar de studenții români, se mizează pe dezvoltarea în echipă și în autonomie a monoposturilor asumate. Evident, comunicarea eficientă între membrii echipei, spiritul critic și competența celor implicați sunt abilități ce se dezvoltă prin intermediul acestei competiții. Mai mult decât atât, prin intermediul acestui concurs, studenții se vor regăsi în situația de a-și răspunde la întrebarea: *„după ce am parcurs în facultate noțiunile teoretice, oare ne pricepem să aplicăm ceea ce am învățat?"*



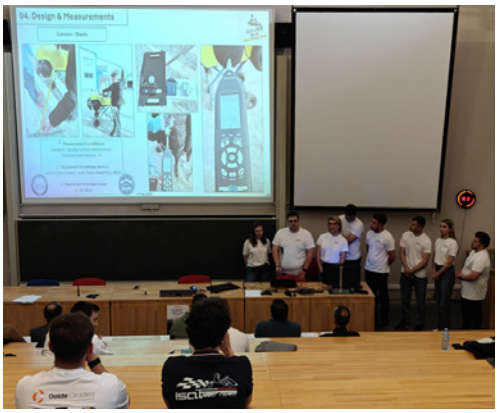
Acum mai bine de 15 ani, aceste idei au fost pe masa discuțiilor fondatorilor acestui concurs. În acea perioadă, ISAT de Nevers și Departamentul Autovehicule și Transporturi al Universității din Pitești puneau bazele acestei provocări (*challenge*) inginerești. Anul acesta, concursul a ajuns la cea de-a 14-a ediție, organizată, pentru a 7 - a oară pe parcursul anilor, de ISAT din Nevers, Franța.





1. *Toate detaliile referitoare la acest caiet de sarcini se regăsesc la http://siar.ro/siar-junior/*









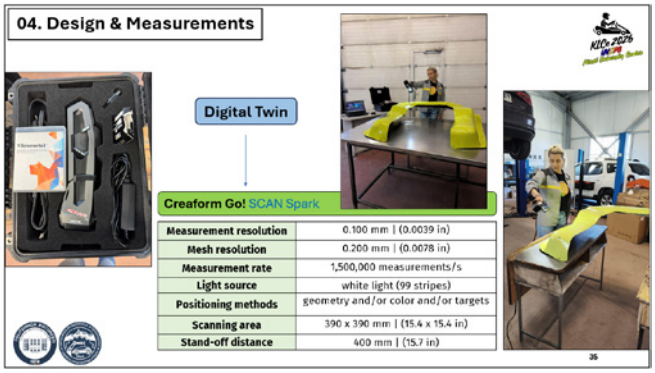
La această a 14-a ediție au participat 40 de studenți: alături de gazde au fost Universitatea Națională de Știință și Tehnologie POLITEHNICA București, Centrul Universitar Pitești și Centrul Universitar București, Universitatea din Oradea și, pentru prima dată intrată în concurs, Ecole Nationale Supérieure des Arts et Métiers (ENSAM) de Cluny, Franța. Astfel, patru echipe de studenți au concurat la componenta „propulsie termică" a competiției și cinci echipe au evoluat în componenta „propulsie electrică".

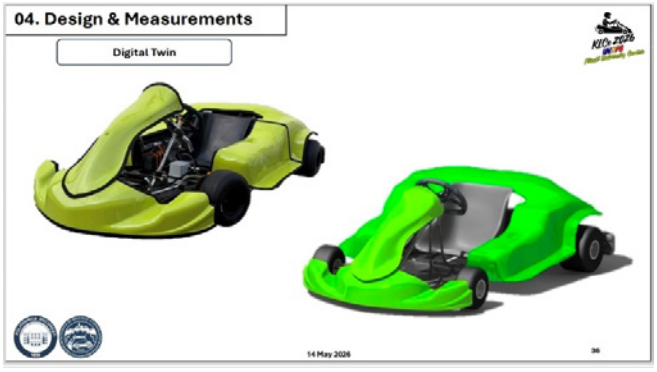
Spre deosebire de alte competiții similare, această provocare inginerească gravitează în jurul ideii de „Low Cost" pentru a *forța* dezvoltarea unor proiecte respectând limite financiare rezonabile care să permită perpetuarea competiției, cu alte cuvinte, implicarea multor studenți, tocmai ca urmare a ideii de competiție *abordabilă* (sub 4000 €, fără TVA, pentru kartul cu motor termic și sub 7500 €, fără TVA, pentru cel electric). Evident, validarea produselor realizate se face concurând pe circuite sportive specifice. Cu alte cuvinte, în cadrul acestei competiții se aduce în prim plan realizarea unui produs funcțional caracterizat de un raport avantajos „performanță (calitate)/preț".

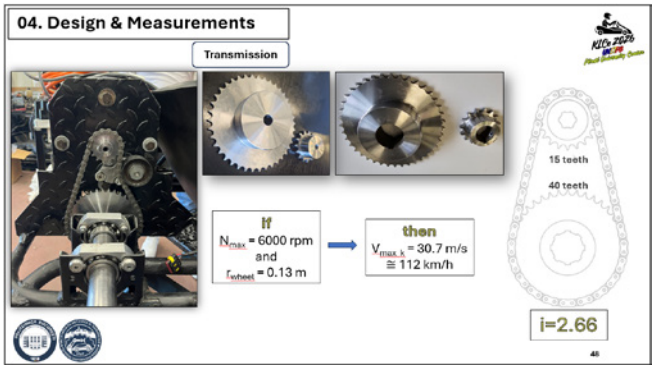
În amfiteatrul ISAT Nevers s-au prezentat 9 proiecte tehnice, studenții punctând detalii ce țin de concepție, proiectare, estetică sau design, fabricare și, nu în ultimul rând, de justificarea încadrării în bugetul impus. Prezentările s-au desfășurat în limba engleză în fața unui juriu mixt, compus din profesorii coordonatori ai echipelor universităților participante.

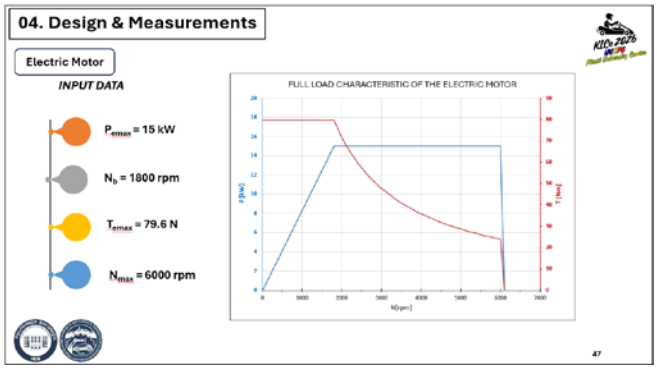
În a doua zi a concursului s-au derulat probele sportive care au constat în calificări, sprint, anduranță și accelerație, unde piloții au demonstrat reale abilități de conducere a karturilor, dar și de rezolvare a problemelor tehnice ce au apărut pe parcursul probelor.











În urma deliberării juriului s-a stabilit un clasament parțial, după prima zi a susținerilor de proiecte inginerești și unul final, după ce, în cea de-a doua zi a concursului s-au cumulat punctajele obținute în prima zi cu punctajele probelor sportive. Nu trebuie să se uite însă că, totuși, participarea în sine, reprezintă și ea o performanță. Astfel, felicităm toți participanții și ne dorim ca acest concurs să aibă din ce în ce mai mulți competitori. Și se demonstrează că suntem pe drumul cel bun ...

Podiumul acestei ediții a fost ocupat de următoarele echipe:

- propulsia termică:
  locul I - Universitatea Națională de Știință și Tehnologie „Politehnica" București, Centrul Universitar Pitești,
  locul II – ISAT de Nevers,
  locul III - Universitatea din Oradea.
- propulsia electrică:
  locul I - Ecole Nationale Supérieure des Arts et Métiers de Cluny,
  locul II - Universitatea Națională de Știință și Tehnologie „Politehnica" București, Centrul Universitar Pitești,
  locul III - Universitatea din Oradea.

Responsabili KLC România:
Adrian-Constantin CLENCI, prof. habil. univ. dr. ing.
Cătălin V. Zaharia, conf. univ. dr. ing.
Universitatea Națională de Știință și Tehnologie Politehnica București,
Centrul Universitar Pitești



REGISTRUL AUTO ROMÂN





















www.autotestmagazin.ro
www.facebook.com/RegistrulAuto
www.facebook.com/autotestmagazin

Programări
la numărul
021/9672
și pe
www.rarom.ro